2009

An investigation into the theoretical and analytical basis for the spread of airborne influenza

John B. Redrow
West Virginia University

An Investigation into the Theoretical and Analytical Basis for the Spread of Airborne Influenza

John B. Redrow

Thesis submitted to the

College of Engineering and Mineral Resources
At
West Virginia University

In partial fulfillment of the requirements for the degree of

Master of Science
In
Aerospace Engineering

Ismail B. Celik, Ph.D., Chair
Eric K. Johnson, Ph.D.
William G. Lindsley, Ph.D.

Mechanical and Aerospace Engineering Department

Morgantown, West Virginia
2009

Keywords: influenza, virus, aerosol, airborne, cough, CFD, droplet

ABSTRACT

An Investigation into the Theoretical and Analytical Basis for the Spread of Airborne Influenza

John B. Redrow

With the threat of a pandemic drawing near and the possibility of a "new", more deadly, form of the influenza virus from genetic re-assortment of avian and human influenza viruses, there is dire need for a better understanding of the transmission mechanisms of this virus. The present study focuses on the aerosol mode of transmission, particularly via the mechanism of human cough. Utilizing computational fluid dynamics (CFD), an in-house code was developed to model the transport of a sputum droplet (cough expectorant) within a jet of air (representative of a human cough). A parametric study was conducted using the model, in order to more thoroughly identify and visualize the conditions that a virus housed within such a droplet would be subject to while in the airborne state. Also, the commercial CFD solver FLUENT was used to perform simulations of an experimental setup at the Morgantown NIOSH facility involving a specialized room containing an apparatus capable of "reproducing" the flow rate and particle size distribution of a human cough. A scenario of a human producing multiple, consecutive coughs within this room was simulated through the use of this software, as well. In these simulations, small particles were injected into the room at the source of the cough, and their trajectories were tracked over time. The calculated particle dispersion within the room was then compared to experimental data to assess the suitability and accuracy of CFD simulations for such a flow.

Acknowledgments

First and foremost, I would like to recognize and express my most sincere appreciation to my advisor, Dr. Ismail Celik. He believed in me and my abilities from the start and has given an abundance of invaluable advice and encouragement, without which I could not have made it this far. I am grateful to my other committee members, Dr. William Lindsley and Dr. Eric Johnson, for all of their help and contributions, as well. I would also like to extend my deepest gratitude to the other members of the CFD group. I have never known a nicer, more generous, or more helpful group of people, and it has been a pleasure working with all of them. Special thanks is due to Ertan, who had the "good fortune" of having a desk right next to mine, and was thus constantly bombarded with questions or problems, but always gave of his time to help. I must again acknowledge Dr. Celik for his exceptional judgment in assembling such a wonderful group, as well. I would also like to acknowledge the help and support of all of my other friends (outside of the lab). Lastly, and above all, I would like to thank my family, particularly my parents, for putting up with me for all these years, and giving their unconditional love and support when I needed it most.

Table of Contents

List of Tables

List of Figures

Nomenclature

c_p	specific heat at constant pressure
D	droplet diameter
D_0	jet initial diameter
D_v	diffusivity of water vapor in air
e_{sat}	saturation vapor pressure over a pure, flat water surface
e_v	partial vapor pressure
$e_{v,0}$	initial vapor pressure of jet
$e_{v,\infty}$	vapor pressure of the ambient
f	drag factor
g	acceleration due to gravity
g_m	growth factor, the ratio of measured diameter to dry diameter of particle
h_L	latent heat of evaporation
k_a	thermal conductivity of air
k_H	ratio of total to mean mass flux
k_M	ratio of total to mean momentum flux
L_v	latent heat of vaporization of water
M	molecular weight
m_s	mass of solute
M_s	molecular weight of solute
Nu	Nusselt number
P	ambient air pressure
Pr	Prandtl number
Q	volume flux
Q_a	vapor density of the ambient air
Q_r	vapor density at the droplet surface
r	droplet radius
R	universal gas constant
RH	relative humidity
r_j	radial coordinate of jet
s	axial distance along buoyant jet centerline
Sc	Schmidt number
Sh	Sherwood number
S_w	water vapor saturation ratio
T	instantaneous droplet temperature
t	time
T_0	initial jet temperature
T_∞	ambient air temperature
T_a	air temperature
T_c	carrier phase temperature; jet centerline temperature
u	continuous phase (air) velocity
v	instantaneous droplet velocity
w	axial velocity of buoyant jet
x	Cartesian coordinate
$x_{s,y}$	mass fraction of component y in the dry solute particle

z	Cartesian coordinate

Greek Symbols

α	entrainment coefficient
Δ_c	effective gravitational acceleration along jet centerline
ε_m	mass fraction of solute with respect to total dry mass
ε_y	mass fraction of component y with respect to total dry mass
η_c	concentration spread rate
η_w	velocity spread rate
θ	jet inclination angle
λ	concentration to velocity width ratio
μ_c	dynamic viscosity of the continuous phase
ν	number of ions into which a solute molecule dissociates
ρ	density
σ	surface tension
τ_T	thermal response time
τ_v	velocity response time
Φ	practical osmotic coefficient
$\omega_{A,\infty}$	mass fraction of species A in the freestream
$\omega_{A,s}$	mass fraction of species A at the droplet surface

Subscripts (unless otherwise included in terms above)

a	air
c	continuous phase property; jet centerline
d	droplet
N	dry particle (e.g. not including water)
s	solution (total droplet)
w	pure water
y	a particular component within droplet

Chapter 1: Introduction to the Problem

1.1 The Influenza Virus and the Threat of Contagion

The influenza virus affects millions of people every year. Currently, there has been widespread concern over a pandemic coming in the near future (Tellier, 2006, Lowen et al., 2006, and Inouye et al., 2006). Coupled with the threat of a human influenza pandemic (possibly of the scale of the Spanish flu of 1918) is the potential for avian influenza (particularly H5N1) to mutate into a form that more easily infects humans. This mutation, or genetic re-assortment, alone could cause a pandemic, as humans will have no immunity to this "new" virus. The Centers for Disease Control and Prevention (CDC) have, in fact, recently identified some North American avian influenza (A H7) viruses that have partially adapted to infect humans (http://www.cdc.gov/media/pressrel/2008/r080610a.htm, 2008). If past cases of human infection with avian flu are any indication as to how deadly this new form will be, then precautionary measures must be taken now to prevent such a plague from occurring. In order to do so, the underlying mechanisms on how influenza is transmitted among the population, and how it infects humans, must be understood.

1.2 Aerosol Transmission of Influenza

There are many who claim that the primary route of transmission of the influenza virus is by large droplets, and that aerosol transmission is negligible, yet there are just as many who disagree with this point of view. In his review of aerosol influenza transmission, Tellier (2006) explains that the epithelial cells of the lower respiratory tract have a certain receptor type that the influenza A virus prefers to bind to, and that the size of particles that exhibit aerosol behavior are of the same order as those that can easily reach the lower respiratory tract upon inhalation. He also cites many other examples as evidence of aerosol transmission, such as the Alaska Airlines outbreak, which involved a defective ventilation system and an unusually high attack rate of influenza. He claims that the 72% attack rate on the plane can only be attributed to higher effectiveness of the aerosol mode of transmission due to a lack of ventilation. After performing experiments on influenza transmission in guinea pigs, Lowen et al. (2006) also concluded that aerosol transmission was indeed possible. In part of their study, they placed the cage of healthy subjects a distance away from the infected guinea pigs, and the uninfected subsequently acquired the virus, however when the relative positions of the two cages were switched there was no transmission—indicating that the airflow in the room had lead to aerosol transmission between cages. In two separate studies on droplet spread in indoor environments and aerosol transmission of infection, Morawska (2006) and Tang et al. (2006) discuss some of the logic behind the argument for airborne transmission as a significant mechanism for the spread of the virus, as well. Our aim in this study is to examine the feasibility of

airborne influenza transmission via small (≤ 10 μm) droplets generated by a human cough.

1.3 Environmental Effects on the Virus

The surrounding environment can have a significant effect on the survival of infectivity of the influenza virus, and knowledge of the factors that affect it the most could provide the key to preventing its transmission. Influenza is an enveloped virus with a diameter of approximately 120 nm (Morawska, 2006 & medicalecology.org, 2004). The envelope is derived from the host cell membrane (composed of phospholipids and proteins), since the virus acquires this envelope as it "buds" from the host cell. Enveloped viruses are generally known to survive better at low relative humidity levels, and at lower temperatures (Sobsey and Meschke, 2003). Polozov et al. (2008) have shown that the lipids of the viral envelope become more ordered as the temperature decreases, which may contribute to better stability of the virus at lower temperatures. Influenza exhibits a particularly interesting trend of survival as a function of humidity—it survives best at low humidity, worst at intermediate humidity, and moderately well at higher humidity (Shaffer et al., 1976 and Lester, 1948). This seems to be directly related to the type of culture the virus was grown in and the suspending medium in which it was aerosolized (Sobsey and Meschke, 2003, Shaffer et al., 1976, and Benbough, 1971). Benbough, after performing experiments with two other enveloped viruses (Langat virus and Semliki Forest virus), showed that the salt content of the suspending medium was the main cause of this "dip" in the survival of infectivity vs. humidity curve (at intermediate humidity).

This could be due to the hygroscopic properties of the salt (which will be discussed in the next chapter), or perhaps to the degradation of the virus lipoprotein by the salt (Lovelock, 1957). Shaffer and Benbough also found that low protein content in the medium lead to a sharp decrease in infectivity from mid to high humidity levels. Shaffer reported the minimum concentration of protein for stability of the virus to be 0.1 mg/mL. Both authors observed that the addition of polyhydroxy compounds to the spraying medium improved stability at mid-range humidity, as well. Inositol, though, has been shown to have a harmful effect at higher humidity, but sucrose and glucose did not (sucrose being more effective than glucose at the same concentration). A few other factors, such as exposure to ultraviolet light, "open air factor" and aerosol particle size, were reported by Sobsey and Meschke (2003) to have an effect on aerosolized viruses. Ultraviolet light is known to inactivate influenza virus, however "open air factor" is poorly defined and it is uncertain what effects this and the aerosol particle size have on influenza's survivability. Stallknecht et al. (1990) studied the effects of pH, salinity, and temperature on avian influenza virus in water. At both 28 C and 17 C, the salinity and pH levels for optimum persistence of the virus had an inverse relationship with each other—persistence was best at zero salt and high pH, but was almost as good at high salt content and low pH (and was worst at high salt/ high pH and low salt/ low pH combinations). Lower temperatures were, of course, proven to be better for the persistence of the virus in the study.

1.4 Literature Review of Related Research

Numerical modeling of the dispersal of droplets generated from expiratory events has been performed in various other studies. Most studies focus on either the transport of larger droplets (diameter > 10 μm) or on the efficiency of different types of ventilation systems at removing airborne contaminant particles. Many of these studies also employ the use of questionable or invalid assumptions or over-simplifications.

In a study on personal exposure to contaminated exhaled air (breath from an infected individual), Bjørn and Nielsen (2002) performed CFD simulations of a breathing thermal (heated) mannequin to estimate the concentrations of contaminant with distance from the mannequin. They used a very simple "box" (rectangular prism) geometry for the mannequin and gave it a square mouth with dimensions of 1.06x1.06 cm. They assumed steady state conditions, with a constant mass flow rate of 3.77×10^{-4} kg/s, corresponding to the maximum instantaneous flow rate of a person breathing.

Sun and Ji (2007) performed a study on the transport and dispersal of droplets produced by coughing, in which they simulated a mannequin producing a cough while in standing, sitting, and supine positions, within a room with displacement ventilation and with mixing ventilation. The mannequin geometry was slightly more complex than in the previous case, having an ellipsoidal head atop a rectangular prism "body". The mouth of the mannequin had a cross-sectional area of 4 cm^2, and was given a velocity boundary condition of 20 m/s over 0.5 s to approximate a cough. Injections (droplets) were set in

the simulations with droplet diameters of 1, 80, and 100 μm (for the case of a horizontally projected cough), with 42,000 droplets of each size. Droplet evaporation was also taken into account until the droplets reached 10% of their original size, at which point it was assumed they had become dry droplet nuclei. In order for evaporation to occur, the energy equation must be solved and the relative humidity of the air must be calculated, as well (as will be seen in Chapter 2). In their simulations, the mannequin body was given a uniform heat flux and the air and droplets coming from the mouth were given a higher temperature and relative humidity than the ambient air. They also performed steady state simulations under the same conditions and showed that a steady state assumption for a cough results in a much greater penetrating length of the coughed air and unrealistic predictions of velocity and distance traveled by the droplets. This assumption, however, may not be as inaccurate for the case of breathing due to the lower velocity of the expired air and the amount of time over which the event occurs.

Another method for modeling the movement and evaporation of a "cloud" of droplets in CFD is to treat the droplet cloud as a continuum phase with one-way coupling to the carrier phase (the air). This was done in a study by Sun et al. (2007), in which the transport equations of a drift-flux model (specifically, equations of the droplet number density and bulk density) are solved as a user-defined scalar, with user-defined functions for the equations of the drift velocity, mass transfer and heat transfer of a single, evaporating droplet, in the commercial CFD software FLUENT. The droplets simulated were composed purely of water, with constant properties specified for the droplet

material. The distribution of 100, 80, and 50 μm droplets within a ventilated, isothermal test room was predicted, assuming steady state conditions within the room.

Wan and Chao (2007) developed a cough-generating apparatus, similar to the "cough machine" developed at NIOSH (described in Chapter 5), in order to study the dispersion of coughed particles. They also performed CFD simulations in FLUENT to compare results with experiments in which the cough generator was placed in a clean-room chamber with different ventilation flow patterns. In their simulations, the cough was produced in the upward direction with a stated airflow rate of 0.4 L/s (the tidal volume of a normal human lung). Again, evaporation of the droplets was taken into account, and pure water was given as the droplet material, with 1.8% non-volatile matter (to act as the dried droplet nuclei). The droplet sizes ranged from 1.5 to 1500 μm, with the size distribution as measured from experiments by Duguid (1946). It is unclear whether or not they assume steady state conditions or if they created an inlet face for the cough generator nozzle exit (where the droplets enter the domain) in the computational geometry, since they do not give any dimensions for this and appear to consistently associate the coughed-air properties to the droplet injection and the droplet properties. To this author, it seems as if they set the conditions for the droplet in the "injections" menu in FLUENT, and were perhaps under the misgiving that the menu was for both the droplets and the air coming from the specified [point] source. If this is the case, then there really is no airflow coming from the source of the "cough" in their simulations, and the stated airflow rate of 0.4 L/s is actually the mass flow rate of the particle stream coming from the injection source.

Xie et al. (2007) modeled the evaporation and movement of a single droplet in a steady-state non-isothermal jet (representative of exhaled air from the mouth), much like the case that is modeled in the present study, however their focus is on larger droplets with initial diameters of 20-200 μm, and they only consider pure water and saline droplets. Also, several assumptions or simplifications are made for some parameters (such as only considering the solute to affect the saturation vapor pressure of water and not accounting for the volume of crystallized solute) which are included or investigated in more detail in the present study.

There are many other studies that could be mentioned here, but for the sake of brevity we will quickly visit just a couple more of the most relevant. Chao et al. (2009) measured the size distribution of expiratory droplets expelled during coughing and during speaking, as well as the velocities of the expiration air jets during these activities. They also performed simulations in FLUENT with a two-dimensional geometry to get a better estimate of the air temperature and relative humidity along the trajectory of the droplets close to the mouth (to a distance of 60 mm away from the mouth). An air velocity of 11.7 m/s was stated for the case of a cough and the mouth diameter was 15 mm. It is presumed that their simulations were steady-state. Tang and Settles (2008) took high-speed schlieren images of a human producing a cough, and mapped the velocity contours from image analysis. One issue that arose upon further review of their results, however, is that the head of the experimental subject is not fixed, and it is seen to tilt during the

cough, which has an effect on the expiratory jet (and therefore invalidates the use of this study for comparison to simulations).

1.5 Objective

Utilizing the powerful tools offered by modern-day CFD, this study aims to elucidate some of the underlying physical phenomena behind the airborne mechanism of transmission of the influenza virus. If we wish to be able to assess the risk of influenza transmission via airborne droplets, we must first learn more about the properties of the droplets themselves and their behavior over time in relation to their surroundings. This will give insight into the conditions to which the virus is being subjected while in transit (within an expiratory droplet). Previous studies have modeled a range of expiratory droplet sizes, usually assuming the droplets to be composed purely of water with constant properties, some including a specified amount of non-volatile matter within the droplet to act as the dry droplet nuclei. For this study, we wish to develop a sophisticated numerical model to study the behavior of a single airborne-size expiratory droplet, with the ability to capture all of the complexity and physical dynamics of such a droplet as occurs in the real-world situation. This level of accuracy is necessary because of the sensitivity of the virus to many different factors, such as the temperature of the surroundings, the relative humidity, droplet salinity, protein and carbohydrate content, etc.

In addition to modeling the smaller scale of a single droplet, and in conjunction with experiments performed at the Morgantown NIOSH facility, the phenomenon of a human cough and the subsequent dispersion of airborne particles (generated by the cough) within a room will be simulated through the use of commercial CFD software. In the NIOSH experiments, a machine "reproduces" a human cough within a non-ventilated (stagnant

air) room, and spectrometers positioned around the room collect and count the particles generated from the "cough" over time. This experimental setup will be re-created in computational domain and simulations will be performed in an attempt to match the experimental particle dispersion with CFD predictions. The case of a mannequin producing multiple, consecutive coughs will also be simulated, in order to better visualize and assess the spread of airborne virus-laden particles from such an event. In contrast to some previous efforts, the current study will incorporate as few assumptions or simplifications as possible, in order to obtain results of the highest accuracy. The flow field in the simulations will be solved under unsteady conditions (as opposed to a steady state assumption), with a transient flow rate prescribed at the source having a profile of flow rate vs. time the same as that of an average human cough (which, consequently, is the same as the flow rate produced by the machine in the experiments). Particles will be introduced at the source for the entire length of the cough, and each particle will be tracked individually in a Lagrangian manner, throughout the domain.

Chapter 2: Characterization of a Sputum Droplet

2.1 Introduction

For this study, we chose to model an aerosol droplet originated from the mouth of a coughing person, as cough is a common symptom of influenza infection, as well as an effective mechanism for spreading the virus. These small droplets are composed of sputum, which is defined as matter which is expectorated from the respiratory tract. Sputum is mostly made up of mucus, though it may contain a small amount of saliva. The human cough can generate as many as 3,000 sputum droplets which will end up as airborne droplet nuclei (Tang, 2006), i.e. the evaporated remains of a droplet (including any pathogens residing within the droplet). For this study, we will focus only on droplets with diameters between 0.4 and 10 μm, since larger droplets tend to fall to the ground due to gravity (thus becoming fomites) and most droplets emitted from a cough are larger than 0.4 micron (Duguid, 1946). Additionally, there would not be very many influenza viruses in a droplet smaller than 0.4 micron due to their size of about 0.1 micron (Murphy & Kingsbury, 1991).

2.2 Interaction of a Water Droplet with its Environment

First, we will look at the simplified case of a pure water droplet in equilibrium with its environment. The droplet can either evaporate or grow by condensation, depending on

the relative humidity and the temperature difference between the droplet and the surroundings. Since relative humidity is defined as the ratio of the partial pressure to the saturation vapor pressure at a given temperature, a droplet will be in equilibrium with its surroundings when these two pressures, as well as the temperature of the droplet and the air, become equal (when relative humidity reaches 100%). On a molecular level, when the partial pressure of a vapor is much higher than the saturation vapor pressure, vapor molecules will form clusters (in the absence of other particles to condense upon, this is called homogeneous nucleation, which will be discussed later). The growth of the clusters will reach equilibrium when the incoming molecular current is equal to the outgoing molecular current at the particle surface. The heat transfer of a particle is mainly due to collisions between host gas molecules. This, in turn, will affect the mass transfer. The rate of the evaporation and condensation, or the rate of heat and mass transport, is governed by diffusion and conduction (Williams and Loyalka, 1991).

From a macromolecular perspective, evaporation or condensation will cause a mass flux over the droplet's surface. Starting with Fick's Law, Crowe et al. (1997) developed a simple equation for the rate of change of mass of a droplet, which relates to the well-known D^2 law (the square of the droplet diameter varies linearly with time). Their formula,

$$\frac{dm}{dt} = Sh\pi D\rho_c D_v\left(\omega_{A,\infty} - \omega_{A,s}\right) \tag{2.1}$$

states that the rate of change of droplet mass is a function of the Sherwood number, Sh (which accounts for the effect of the relative velocity between the droplet and the gas), droplet diameter, D, density of the carrier phase, ρ_c, diffusion coefficient, D_v, and mass

fractions of the species in the freestream and at the droplet surface, $\omega_{A,\infty}$ and $\omega_{A,s}$. For the conservation of momentum, the forces acting on a droplet are equal to the sum of the momentum flux through the surface and the rate of change of momentum within the control volume. These forces can be subdivided into body and surface forces, such as gravity and drag. The energy equation for a droplet with mass transfer,

$$\frac{dT_d}{dt} = \frac{Nu}{2}\frac{1}{\tau_T}(T_c - T_d) + \frac{Sh}{2}\frac{1}{\tau_T}\frac{\Pr}{Sc}\frac{h_L}{c_p}(\omega_{A,\infty} - \omega_{A,s}) \tag{2.2}$$

states that the temperature change over time is a function of the Nusselt number, Nu, thermal response time, τ_T, temperature difference between the carrier phase and droplet, the Sherwood number, Prandtl number, $\Pr$, Schmidt number, Sc, latent heat, h_L, specific heat of the carrier phase, c_p, and the mass fraction difference at the droplet surface and in the freestream. While the droplet is evaporating or condensing, the temperature will remain constant (once the "wet bulb" temperature has been reached) and the heat transfer will balance the energy needed for the change of phase.

2.3 Chemical Components of Sputum and their Effects in Binary Aqueous Solutions

Human airway mucus is made up of about 95% water, 2% glycoprotein, 1% protein, 1% lipids, and 1% inorganic salts (Samet and Cheng, 1994). A more complex breakdown of the chemical composition of sputum and the composition of tracheobronchial secretions is given in Tables 2.1 and 2.2 (data from Spicer and Martinez, 1984). Here, we will look at the hygroscopic properties of each individual chemical constituent in order to develop

a better understanding of how the sputum droplet will behave in the ambient environment.

Table 2.1: Composition of purulent and non-purulent human sputum

Composition	***mg/mL***	***mg/mL***	***SD (purulent)***
	Nonpurulent	*Purulent*	
Water	954.000	934.000	12
Macromolecular dry weight	46.000	60.000	8.6
Protein	12.100	19.900	4.6
Lipid	10.600	18.100	2.7
Carbohydrate	9.200	12.300	1.4
DNA	0.008	0.820	0.28
Total	985.908	985.120	29.58

Table 2.2: Chemical composition of human tracheobronchial secretions

Composition	***% of dry weight***
Total Protein	33.80
Total lipid	12.30
Phospholipid	5.70
PS	1.04
PI	0.01
PE	1.47
PC	3.18
Neutral lipid	6.97
Glycolipid	1.78
Total carbohydrate	48.90
D-Ribose	1.01
Ribose	0.08
Mannose	3.28
Glucose	2.54
Fucose	5.82
Galactose	10.37
N-CHO (amino sugars)	14.87
Sialic acid	10.93
Glycoprotein	33.27
Protein	1.00
Fucose	1.21
Galactose	0.87
H-CHO	1.67
Sialic acid	1.54
Sulfate	0.41

We first look at the saline droplet (salt + water) assuming that all of the salt content is sodium chloride. The dissolution of salt in water will lower the surface vapor pressure of the water. Thus, the term "water activity" is used instead of "relative humidity" to relate this property of a solute in an aqueous solution (at equilibrium). A saturated sodium chloride solution has a water activity of about 0.75 (Tang, 1979). This is called the deliquescence relative humidity, or the humidity at which a dry NaCl particle will suddenly become a (saturated) saline droplet. The process is not reversible, however—the saline droplet will not effloresce (crystallize) unless the relative humidity reaches about 45% or lower. This is known as hysteresis, or path-dependency, since one cannot simply predict the droplet's behavior at any instant, unless the history is known. The reason for this will be discussed in the next section.

The carbohydrate content is considered to be solely glucose, since its properties are well-documented, and it is present in a significant amount in sputum. Like salt, glucose is also hydrophilic, and will lower the surface vapor pressure, as well. Glucose has a deliquescence relative humidity of about 89%, much higher than sodium chloride. It does not, however, have a distinct efflorescence point—the absorption or water loss with a change of humidity seems to be reversible. Experiments have shown it to be completely free of water around 10% to 20% relative humidity (Peng et al., 2001).

For simplicity, and because albumin is one of the main proteins in airway secretions (Majima et al., 1999), the protein content of the droplet will be modeled as bovine serum albumin (BSA), a well-defined protein that is often used in experimental studies

(Mikhailov et al., 2004). In their study, Mikhailov et al. regard BSA as a completely soluble protein, and find that it has a reversible growth vs. relative humidity curve (like glucose), with efflorescence/deliquescence at about 35% relative humidity.

The lipid content of the sputum droplet will be modeled as phosphatidylcholine (PC), the main phospholipid found in sputum (Spicer & Martinez, 1984). Its properties have been reported in numerous studies (Mansour et al., 2001, Schrader et al., 2002, and Tanaka et al., 1986). Phosphatidylcholine is an amphiphilic molecule, since it is composed of a hydrophobic "tail" and a hydrophilic "head". Therefore, PC acts as a surfactant in water, and the molecules form a layer at the air-water interface, with the hydrophobic part out of the water, and the hydrophilic portion in the water. This is called a monolayer (or, more specifically, a "Langmuir monolayer"), and is known to significantly lower the surface tension of water (Langmuir, 1917, Wustneck et al., 2005, and Mudgil et al., 2006). Experimental studies have also shown that a monolayer can have a large effect on the evaporation rate of water, in some cases reducing it by as much as 70-75% (Frenkiel, 1965). Lozato et al. (2001) reported an even larger reduction of evaporation, 90-95%, due to the meibomian lipid layer in their studies of the human eye.

2.4 Solute Nucleation

Nucleation is a term used to describe the point at which a supersaturated solution forms a "nucleus" of the solid phase of the solute. A system that is supersaturated is said to be in a metastable state (Carey, 2007). As the system goes further into the metastable range, it

becomes more probable that a large enough perturbation will occur to cause a phase transition. If a localized density fluctuation causes the state to exceed the stability limits, then it will result in the formation of a small "embryo" of another phase. These embryos can be stable or they may be unstable, in which case they will either collapse or grow. If they grow, it will result in rapid nucleation of the system (crystallization). There are two types of nucleation – heterogeneous and homogeneous. Heterogeneous nucleation occurs when there are foreign surfaces or foreign ions present, which serve as nucleation sites, catalyzing the formation of the new phase. Homogeneous nucleation occurs when the new phase is initiated all by itself, directly from the solution, and therefore requires much higher supersaturations (Cohen, 1987). Often, homogeneous nucleation is assumed for aerosol droplets, as they lack the presence of a foreign surface to induce nucleation. Thus is explained the hysteresis observed in saline droplets (and the large difference between the efflorescence and deliquescence relative humidity) – it is due to the non-equilibrium condition of supersaturation in the droplet. If heterogeneous nucleation were the case, the efflorescence relative humidity would be much closer to the deliquescence relative humidity.

2.5 Interactions Between Components in a Sputum Droplet

The analysis of a multi-component aqueous droplet is further complicated by the intricate interactions between the various constituents in the droplet, and their combined effect on the evaporation (or growth) of the droplet. For solutions containing only electrolytes, there are many models available to predict the overall activity coefficient (which can be

used to find the water activity), most notably the Pitzer and Debye-Huckel models. For non-electrolyte solutions, UNIFAC is a well-known and tested model. As yet, however, there is no accurate, widely accepted model to predict the behavior of a droplet containing electrolyte and non-electrolyte solutes, as well as insoluble compounds. The Zdanovskii-Stokes-Robinson relation is not being considered here since it is only applicable to ideal solutions, when solute-solute interactions are negligible (this is not our case, as will be described next). So, here we will attempt to obtain a better idea of how a sputum droplet will behave in the atmosphere by studying some of the interactions of the constituents in ternary solutions.

Mikhailov et al. (2004) performed a study on the interaction of protein and salt aerosol particles with water vapor. For mixed NaCl—BSA particles, the measured mobility diameter showed a significant decrease as the relative humidity approached the deliquescence point, most noticeably with a dry mass fraction of 25% BSA. With increasing percentages of BSA, the deliquescence and efflorescence transitions seem to become less sharp, and the humidity at which efflorescence occurred decreased. The authors suggest that the BSA may form a coating on the surface of the droplet (since proteins tend to act as surfactants) and "limits the access of water vapor to the particle core composed of NaCl." Investigating this phenomenon further, the authors state that the particles with a high BSA percentage have a near-spherical envelope with a dendritic NaCl core, and they assert that the BSA matrix forms a diffusion barrier which inhibits the formation of compact NaCl crystals. This is to say that BSA kinetically limits the deliquescence and efflorescence of NaCl.

The authors claim, however, that this is not enough to explain the large differences in diameter between mixed particles and pure NaCl particles under the same conditions. The authors hypothesize that electric charge effects may be the reason, since BSA molecules carry a high number of elementary charges, and at neutral pH they have a negative net electric charge that depends on the amount of salt ions in the solution. This, they say, caused enhanced electrostatic repulsion between the BSA molecules, which then formed porous agglomerates. The agglomerate structure was subsequently compacted by capillary condensation or deliquescence and efflorescence.

The water activity of glucose + sodium chloride solutions was determined by Comesana et al. (1999). They also find the value for the C_{12} coefficient in the equation proposed by Lin et al. (1996): $a_w - 1 = (a_{w1} - 1) + (a_{w2} - 1) + C_{12} m_1 m_2$, where a_w is water activity, m is molality, and 1 and 2 refer to glucose and sodium chloride, respectively.

Chapter 3: Single Droplet Mathematical Model

3.1 Introduction

Utilizing computational fluid dynamics (CFD), a model has been created to study the spread of airborne influenza. A single, evaporating sputum droplet in a time-averaged turbulent buoyant jet (representative of a human cough) has been simulated in MATLAB. The output of this model includes the variation of the droplet's size, temperature, velocity, and concentration of constituents over time. These constituents include salt (NaCl), carbohydrate, protein, lipids, and DNA content—the same chemical components found in sputum. The initial concentration of any particular component can be specified, and measured "actual" physiological amounts can be found in the literature (Spicer & Martinez, 1984). The initial temperature, relative humidity, and velocity of the jet and the temperature and relative humidity of the stagnant ambient into which it issues can all be set, as well. Lastly, the droplet's initial size and temperature can be specified in the program. The droplets simulated will have [initial] diameters between 1 and 10 microns.

3.2 Droplet Radius, Temperature, and Velocity Change with Time

Following the model used by Pruppacher and Klett (1978) for the evaporation or condensation of an aqueous solution droplet, the rate of change of droplet radius is:

$$r\frac{dr}{dt}=\frac{D_v M_w e_{sat}(T_a)}{\rho_s R T_a}\left\{RH-\frac{1}{1+\delta}\times\exp\left[\frac{L_v M_w}{RT_a}\left(\frac{\delta}{1+\delta}\right)+\frac{2M_w\sigma_s}{RT_a(1+\delta)\rho_w r}-\frac{\nu\Phi_s m_s\left(M_w/M_s\right)}{\left(4\pi r^3\rho_s/3\right)-m_s}\right]\right\} \tag{3.1}$$

Where:

$$\delta=\frac{T}{T_a}-1=\frac{L_v\rho_s}{T_a k_a}r\frac{dr}{dt} \tag{3.2}$$

In the above equations, r is the droplet radius, t is time, D_v is the diffusivity of water vapor in air, M is molecular weight, T_a is the ambient air temperature, e_{sat} is the saturation vapor pressure over a pure, flat water surface at temperature T_a, ρ_s is the [total] density of the droplet, ρ_w is the density of pure water (at droplet temperature), R is the universal gas constant, RH is the relative humidity (as a decimal), L_v is the latent heat of vaporization of water, σ is the surface tension, ν is the number of ions into which a salt molecule dissociates, Φ is the practical osmotic coefficient, m is mass, T is the instantaneous droplet temperature, and k_a is the thermal conductivity of air. The subscripts w and s stand for water and [solution] droplet, respectively. Note here that the nomenclature used in this study is not the same as that of Pruppacher and Klett. The temperature of the droplet is assumed to be uniform, an assumption which has been validated in the literature (Andreas, 1990). It is also assumed that the droplet is initially spherical and mass exchange is uniform over the surface of the droplet, thus it will always remain

spherical. Equation (3.1) is an implicit equation due to the dependence of δ on r. In our model, the previously calculated value of T is used to determine δ, which can be justified by the fact that the time scale for the change in droplet temperature is much smaller than the time scale for a change in droplet radius. Note that Equation (3.2) is an approximation assuming that the latent heat of evaporation is equal to the heat conduction at the droplet surface (i.e. a Nusselt number of 2 is assumed when determining the total heat flux, implying that the droplet is in a stagnant medium with no forced or free convection effects) and cannot be used to replace Equation (3.1).

The rate of change in droplet temperature is modeled by (Pruppacher and Klett, 1978):

$$\frac{d}{dt}\left(T_a - T\right) = \frac{-3}{r^2 \rho_s c_{ps}}\left[k_a\left(T_a - T\right) + L_v D_v\left(Q_a - Q_r\right)\right] \tag{3.3}$$

Where:

$$Q_r = \frac{100 M_w e_{sat}\left(T\right)}{RT} \exp y_{\text{var}} \tag{3.4}$$

And:

$$y_{\text{var}} = \frac{2 M_w \sigma_s}{R T_a \rho_w r} - \frac{\nu \Phi_s m_s \left(M_w / M_s\right)}{\left(4\pi r \rho_s / 3\right) - m_s} \tag{3.5}$$

Here, c_{ps} is the specific heat of the droplet at constant pressure, and Q_a and Q_r are the vapor density of the ambient air and at the droplet surface, respectively.

The equation of motion for a particle, using the steady-state drag coefficient and including the effect of buoyancy, is given by Crowe, Sommerfeld, and Tsuji (1997):

$$\frac{d\vec{v}}{dt} = \frac{f}{\tau_v}(\vec{u} - \vec{v}) + \vec{g}\left(1 - \frac{\rho_c}{\rho_d}\right) \tag{3.6}$$

where:

$$\tau_v = \frac{\rho_d D^2 C_c}{18\mu_c} \tag{3.7}$$

In the equations above, v is the droplet velocity (vector), f is the drag factor, u is the velocity of the continuous phase, τ_v is the velocity response time, g is the acceleration of gravity, ρ_c is the density of the continuous phase, ρ_d is the droplet density, D is the droplet diameter, C_c is the Cunningham slip correction factor, and μ_c is the viscosity of the continuous phase. An empirical formula, given by Clift and Gauvin (1970) is used for the drag factor:

$$f = 1 + 0.15\,\mathrm{Re}^{0.687} + 0.0175\,\mathrm{Re}\left(1 + 4.25\times10^4\,\mathrm{Re}^{-1.16}\right)^{-1} \tag{3.8}$$

where Re is the Reynolds number based on the relative velocity. This formula is valid across the entire subcritical Reynolds number range ($Re<3*10^5$). It can be shown that the relative velocity between the droplet and the continuous phase would have to be very large (in the order of 10^5 m/s) to exceed this range (for smaller, airborne droplets which we are interested in). The Cunningham slip correction factor, a correction for the momentum of very small droplets within a Stokes flow regime (Re<1) is given by:

$$C_c = 1 + \frac{2\lambda_L}{D}\left[1.257 + 0.4\exp\left(\frac{-0.55D}{\lambda_L}\right)\right] \tag{3.9}$$

where λ_L is the mean free path of the molecules, taken as $7*10^{-8}$ meters.

Andreas (2005) has compiled functions for calculating many dynamic and thermodynamic variables in a very convenient handbook. Most of the parameters in the equations above can be determined from the empirical formulas given in this reference.

3.3 Modification for Multiple Component Droplet

The above formulations work for a single solute droplet, but for our purposes we need a model that can handle multiple components, soluble and insoluble alike. To do so, we must modify the given model. By combining the surface vapor relation for an aqueous droplet containing a solid substance (Pruppacher & Klett, 1978):

$$\frac{e_a}{e_{sat,w}} = \exp\left[\frac{2M_w\sigma_s}{RT\rho_w r} - \frac{\nu\Phi_s\varepsilon_m M_w\rho_N r_N^3}{M_s\rho_w\left(r^3 - r_N^3\right)}\right] \tag{3.10}$$

And the same correlation from Mikhailov et al (2004) for an aqueous droplet containing multiple solutes which do not interact with one another (separate solute volume additivity model):

$$S_w = \exp\left(\frac{4\sigma M_w}{\rho RTD} - \frac{M_w}{\rho_w\left(g_m^3 - 1\right)}\sum_y \frac{\nu_y\Phi_y\rho_y x_{s,y}}{M_y}\right) \tag{3.11}$$

Replacing the last term in the droplet radius equation with the result, we end up with:

$$r\frac{dr}{dt} = \frac{D_v M_w e_{sat}(T_a)}{\rho_s RT_a}\left\{RH - \frac{1}{1+\delta}\times\exp\left[\frac{L_v M_w}{RT_a}\left(\frac{\delta}{1+\delta}\right) + \frac{2M_w\sigma_s}{RT_a(1+\delta)\rho_w r} - \frac{M_w\rho_N r_N^3}{\rho_w\left(r^3 - r_N^3\right)}\sum_y \frac{\nu_y\Phi_y\varepsilon_y}{M_y}\right]\right\} \tag{3.12}$$

In the above modification, ε is the mass fraction of a constituent with respect to the total dry mass, the subscript N refers to the dry particle, and the subscript y refers to a

particular constituent of the particle. The variable y_{var} will also be changed to the natural log of the surface vapor relation given above.

3.4 Buoyant Jet Momentum and Temperature

The droplet will be issuing from the mouth of a coughing person, into stagnant ambient surroundings. Therefore, a round buoyant jet must be added to the model, as it will give the conditions immediately surrounding the droplet. Here, the model given by Wang, Law, and Herlina (2003) was chosen.

For the momentum and buoyancy fluxes:

$$\frac{d}{ds}\left(0.5k_M w_c^2 \eta_w^2 s^2 \sin(\theta)\right) = \Delta_c \lambda^2 \eta_w^2 s^2 \tag{3.13}$$

$$\frac{d}{ds}\left(k_M w_c^2 \eta_w^2 s^2 \cos(\theta)\right) = 0 \tag{3.14}$$

$$\frac{d}{ds}\left(k_H \frac{\lambda^2}{1+\lambda^2} w_c \Delta_c \eta_w^2 s^2\right) = 0 \tag{3.15}$$

With the trajectory defined as:

$$\frac{dx}{ds} = \cos(\theta) \tag{3.16}$$

and

$$\frac{dz}{ds} = \sin(\theta) \tag{3.17}$$

For the volume flux:

$$\frac{dQ}{ds} = 2\pi\alpha\eta_w s w_c \tag{3.18}$$

In the above, s is the axial direction cylindrical coordinate, k_M and k_H are the ratios of total to mean momentum and mass flux, respectively, w_c is the velocity along the centerline of the jet in the s-direction, η_w is the velocity spread rate, θ is the inclination angle, Δ_c is the effective gravitational acceleration along the centerline, λ is the concentration to velocity width ratio, x and z are the Cartesian coordinates, and α is the entrainment coefficient.

The centerline temperature at any point along a jet is given by Bejan (2004). The expression used is:

$$T_c = 5.65\frac{(T_0 - T_\infty)D_0}{s} + T_\infty \tag{3.19}$$

Here, T_0 is the initial jet temperature, T_∞ is the ambient air temperature, and D_0 is the nozzle (mouth) diameter.

The temperature at any point is then:

$$T_a = \left(T_c - T_\infty\right)\exp\left[-\left(\frac{r_j}{\eta_c s}\right)^2\right] + T_\infty \tag{3.20}$$

The axial velocity at any point is given by:

$$w = w_c \exp\left[-\left(\frac{r_j}{\eta_w s}\right)^2\right] \tag{3.21}$$

The relative humidity at any point is:

$$RH = \frac{e_v}{e_{sat}} \tag{3.22}$$

Where the saturation vapor pressure is given empirically by Buck (1981):

$$e_{sat} = 6.1121*\left(1.0007 + \left(3.46e-06\right)P\right)\exp\left(\frac{17.502T_a}{240.97 + T_a}\right) \tag{3.23}$$

And an expression for the partial vapor pressure was developed:

$$e_v = \left(\frac{T_a - T_\infty}{T_0 - T_\infty}\right)e_{v,0} + \left(1 - \frac{T_a - T_\infty}{T_0 - T_\infty}\right)e_{v,\infty} \tag{3.24}$$

Above, r_j is the radial coordinate, η_c is the concentration spread rate, P is the ambient air pressure, $e_{v,0}$ is the initial vapor pressure of the jet, and $e_{v,\infty}$ is the vapor pressure of the ambient air. For clarity, and as a visual aid, a two-dimensional diagram of the buoyant jet (with imaginary boundaries) is included below, in Figure 1. Profiles of the jet axial

velocity (solid line) and temperature difference between the jet and the ambient air (dashed line) at an axial distance far downstream of the inlet are also shown in the figure.

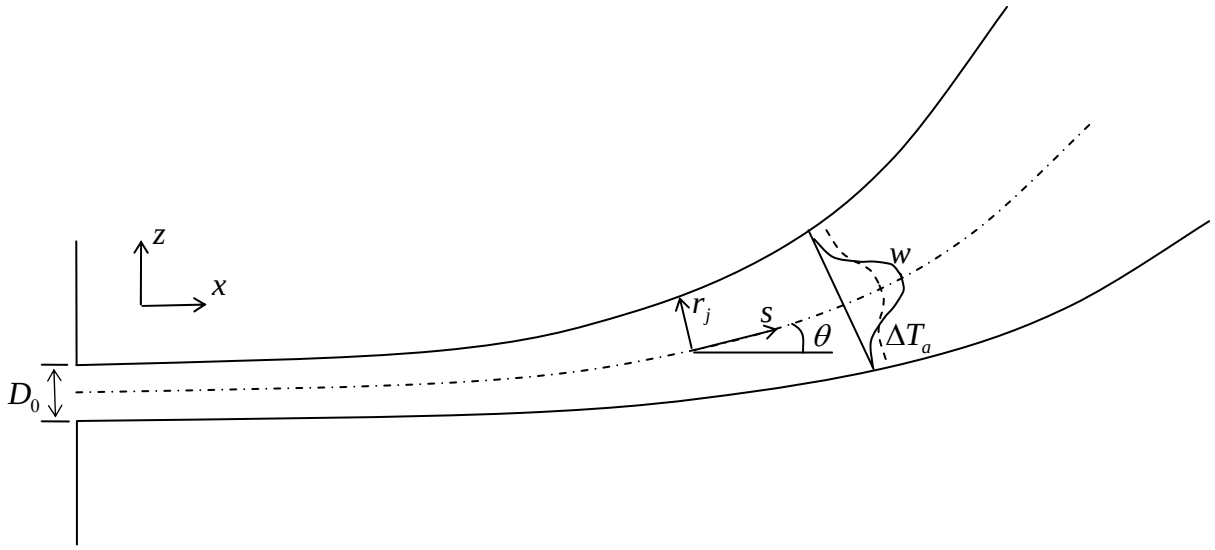

Figure 1: Sketch of buoyant jet in two dimensions, with temperature and velocity profiles.

Chapter 4: Results from Single Droplet Simulation

4.1 Introduction

Here, we present some of our model's predictions from each step of the modeling process, beginning with the case of a droplet of pure water in a steady, uniform environment, then adding the effects of the buoyant jet and solutes within the droplet, and finally ending up with a droplet composed of the same constituents as are found in human sputum. We also compare our results with experimental data in order to validate our model and the assumptions that were made. In the model, it was assumed that the droplet is initially spherical in shape and it will always remain spherical, the droplet temperature at any given instant will be uniform, and any constituents contained within the droplet are well-mixed. Through these assumptions, it is implied that the evaporation or condensation over the droplet surface will be uniform, and that a solution droplet will always have uniform density, as well. Since there is no well-accepted, accurate, and widely-applicable method for calculating the surface tension of multi-component solutions, and since the surface tension term in equation 3.12 is only significant for sub-micron sized droplets (becoming more significant with decreasing radius), we assume the droplet to have a surface tension equal to that of pure water. To check this assumption, we tested our model with the droplet surface tension set at zero and at eighty dynes/cm and found the difference in the results to be negligible.

4.2 Pure Water Droplet Evaporation

Since sputum is mostly comprised of water, we initially created a model based on the relations given by Crowe et al. (1997) to capture the physics of a droplet of pure water, placed into an environment (of air) with a given (constant) relative humidity, temperature, and velocity. Using a Lagrangian, forward-stepping time-marching approach to solve the coupled ODE's for the droplet diameter, velocity, and temperature, this model was able to accurately predict the change in these three parameters over time. The results for the change in particle diameter at different values of relative humidity for 1, 10, and 100 μm droplets, shown below in Figure 1, were validated by comparing with those of Morawska (2006).

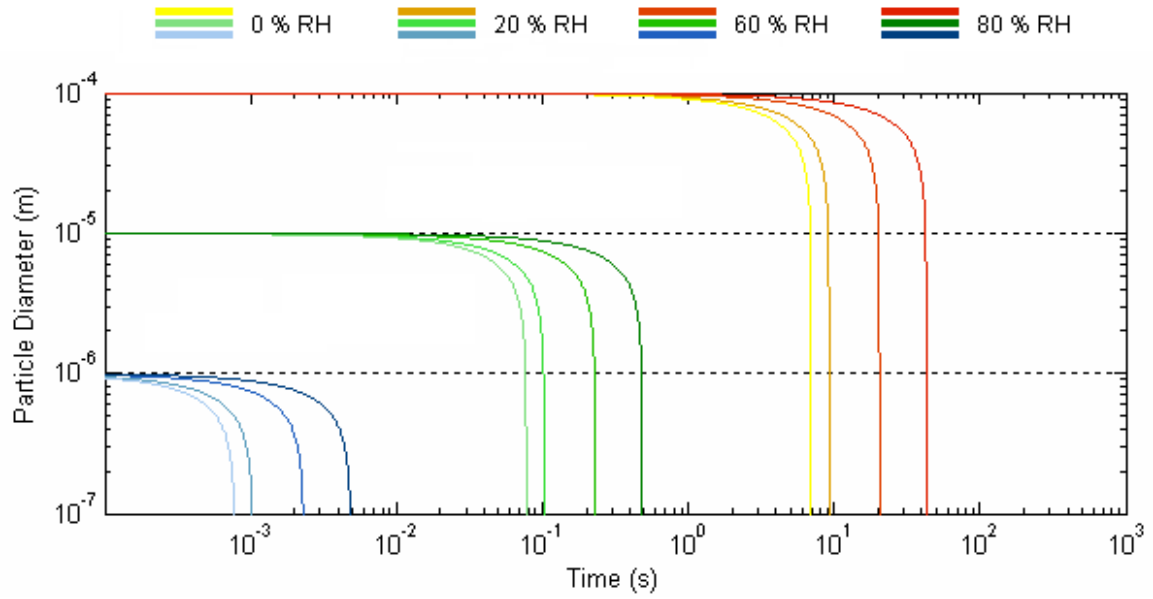

Figure 2: Particle diameter change with time of evaporating water droplets in different ambient conditions.

Different initial conditions for the droplet and the ambient air in the room can be shown to have drastically different effects on the droplet's behavior. The droplet can evaporate

completely, evaporate some and then remain at whatever size it reached, grow by condensation until it reaches an equilibrium size, or it can even grow some initially and then evaporate completely. These different effects are illustrated in Figure 2 with a 1 micron droplet at different initial temperatures (Td), in an environment of a specified relative humidity and a constant ambient temperature of 296.15 °K. Figure 3 is a plot of the particle (droplet) temperature over time, corresponding to the same droplets in Figure 2. It can be observed from this figure that a droplet of this size will reach its wet bulb temperature (the temperature at which an evaporating or condensing droplet is in equilibrium with its surroundings) in a very short time, almost instantaneously, and will remain at this temperature indefinitely, as long as the conditions of the surroundings are not changed, or until the droplet has completely evaporated.

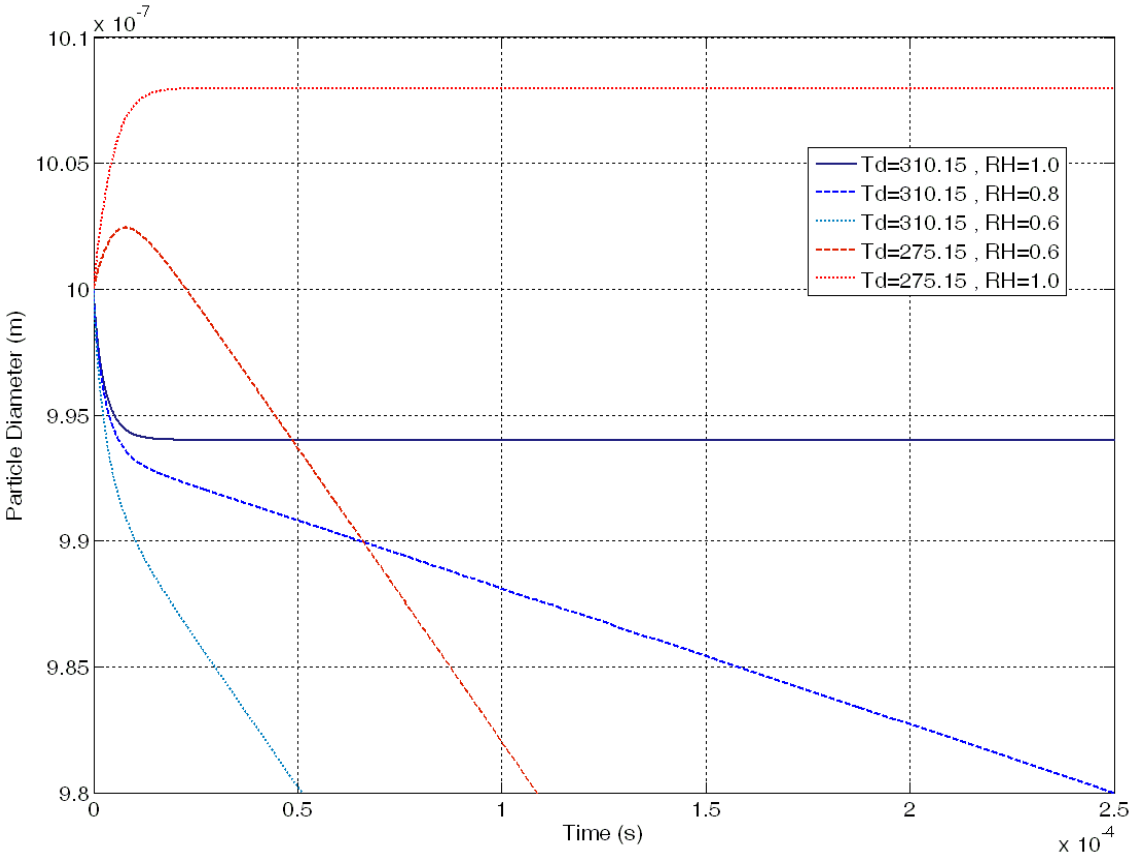

Figure 3: Droplet diameter change with time of 1 micron droplets under different conditions.

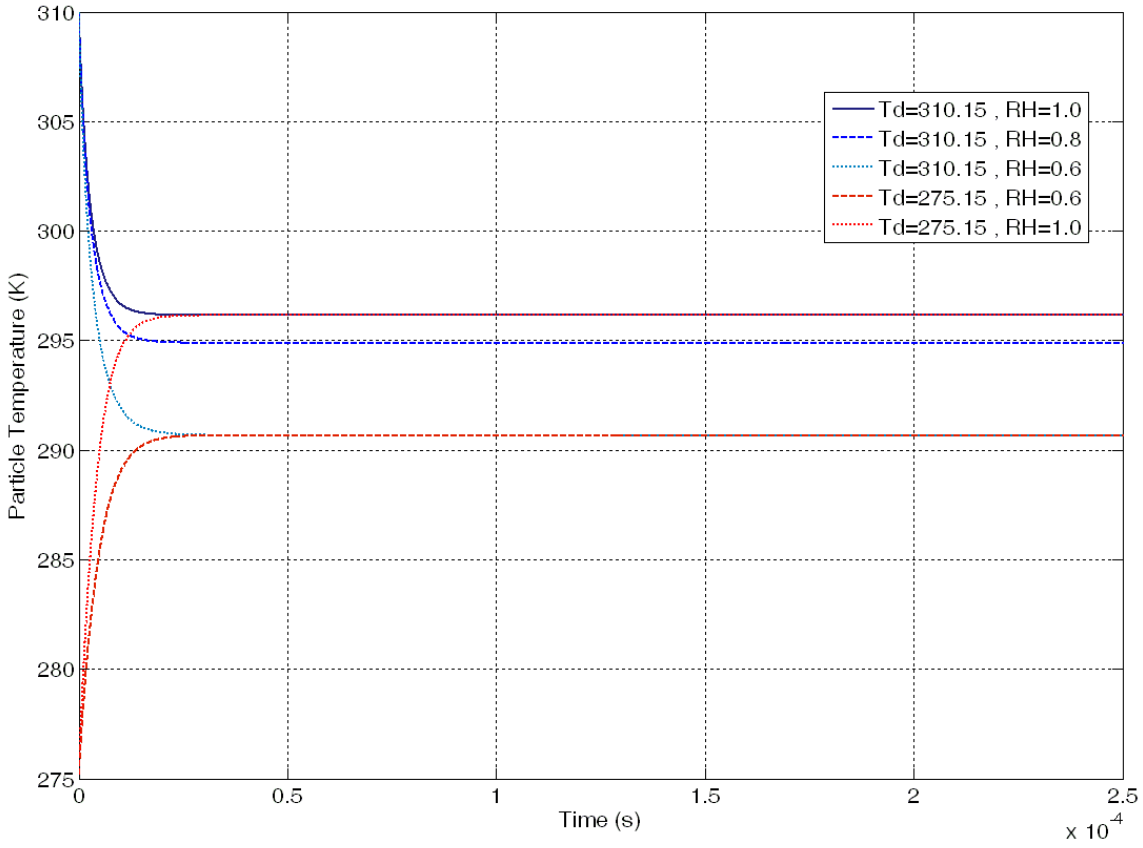

Figure 4: Droplet temperature change with time of 1 micron droplets under different conditions.

4.3 The Buoyant Jet

Since the air leaving the mouth of a coughing person should be at a higher temperature, relative humidity, and, of course, velocity, than the air in the room, it can be modeled as a jet of air with buoyancy. The details of this part of the modeling are described in Chapter 3. To give a better visualization of what this time-averaged turbulent buoyant jet looks like under different conditions, Figures 4 and 5 show contours of the temperature and velocity, respectively, on a vertical slice through the center of the jet. The initial jet velocity is 2 m/s in Figure 4 and 10 m/s in Figure 5. The initial jet temperature is 310.15

°K and the ambient temperature is 294.15 °K in both figures. Figure 6 shows the effect of changing the jet velocity on a particle introduced at the center of the "mouth".

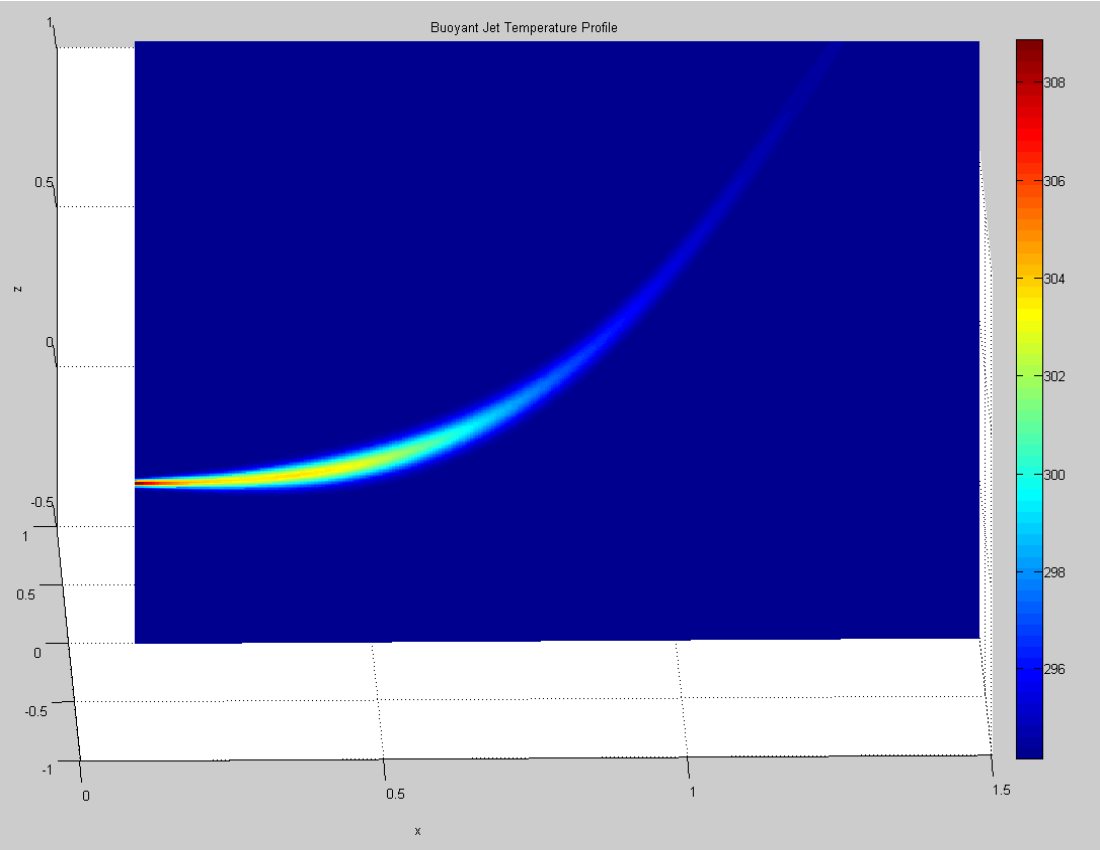

Figure 5: Temperature contour on a slice through the center of the buoyant jet.

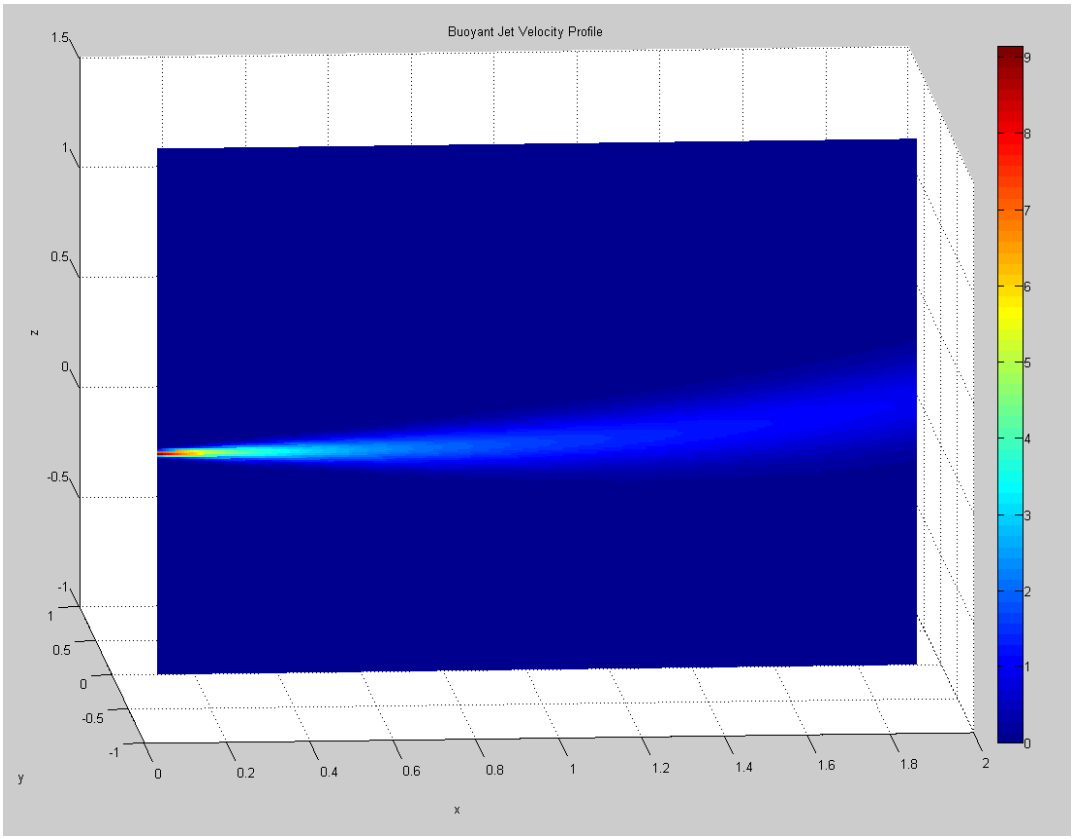

Figure 6: Contours of velocity on a slice through the center of the buoyant jet.

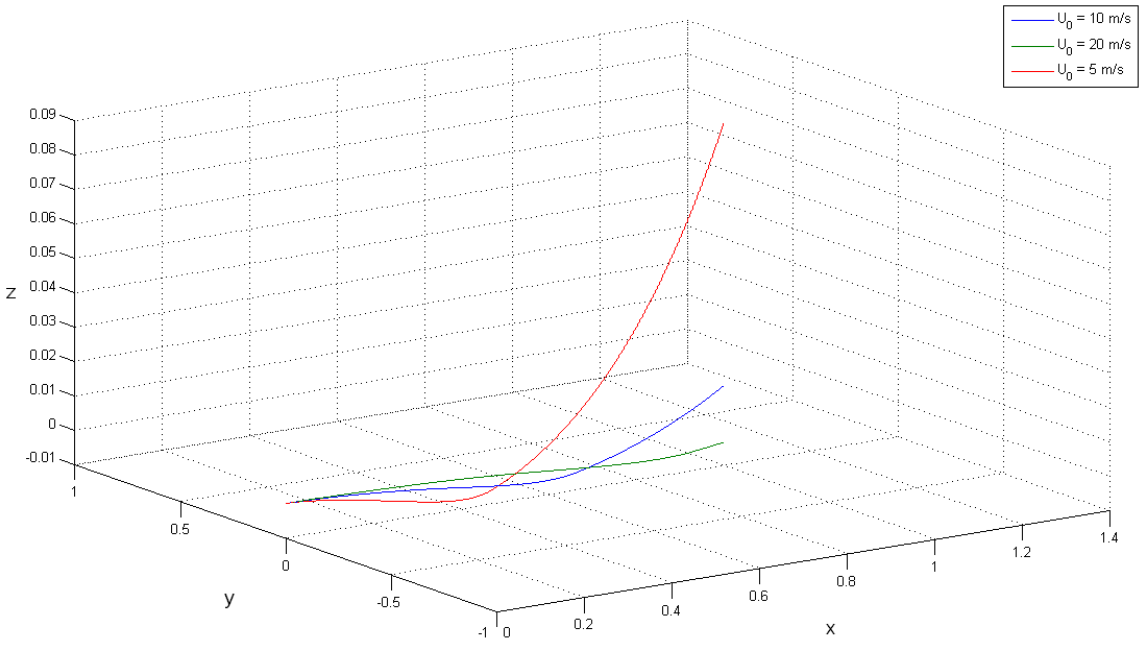

Figure 7: Trajectories of a particle initialized at the center of the buoyant jet with different initial jet velocities (U_0).

Due to the fact that the jet is initially at a different temperature and humidity than the ambient environment, and proceeds to mix with the air in the room, the temperature and humidity of the air immediately surrounding the droplet can change with time and space. This will, of course, change the way the droplet evaporates or grows, as illustrated in Figure 7. Note that the subscripts 'a' and 'j' in the figure legend stand for ambient and jet, respectively. The droplet diameter vs. time and temperature vs. time were plotted both linearly and logarithmically in time to better capture the magnitude of the changes.

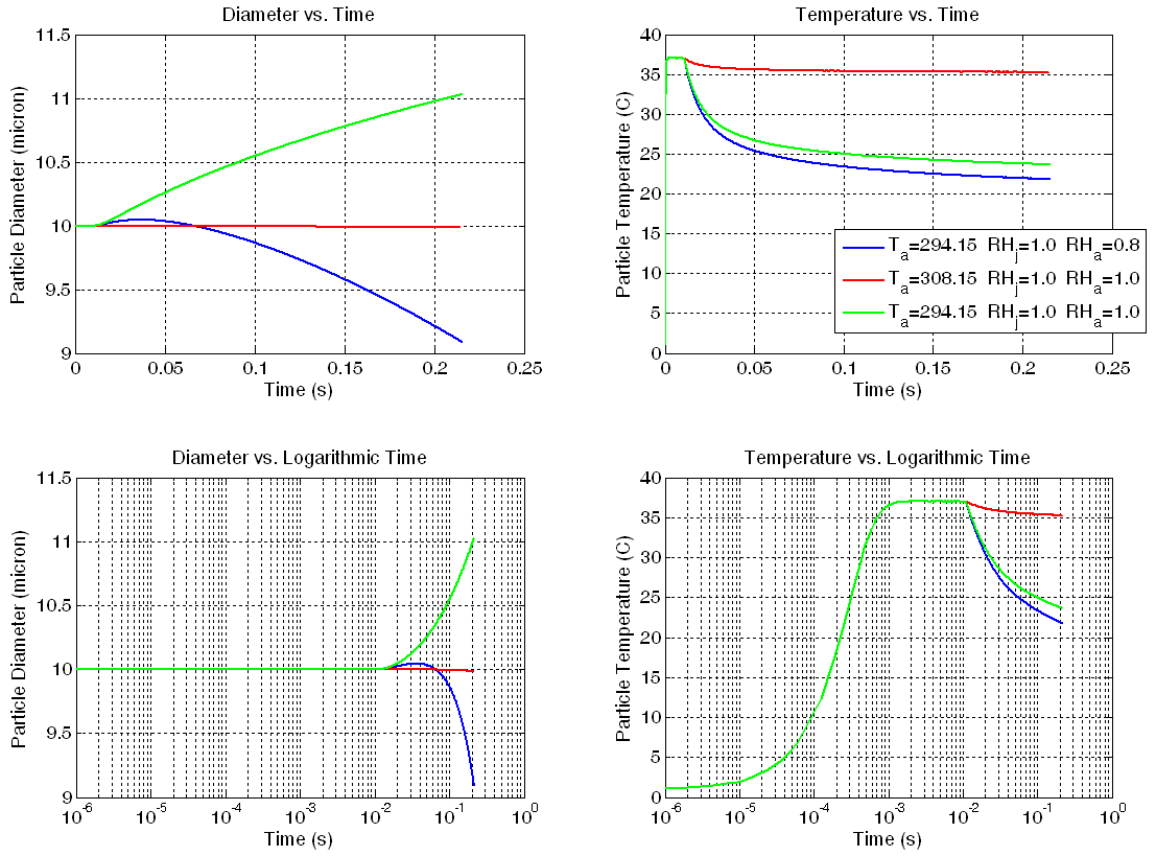

Figure 8: Droplet behavior in buoyant jets with differing ambient temperatures and values of relative humidity.

4.4 Single-Solute Droplet Behavior

Solutes contained within an aqueous droplet can have a large effect on its behavior due to their hygroscopic nature. The solutes dissolved within a droplet will change the surface vapor pressure, and some, such as sodium chloride, exhibit the phenomena of efflorescence and deliquescence. Figure 8 compares the evaporation of a 10um droplet of pure water to that of droplets with differing salinity (different initial concentrations of NaCl).

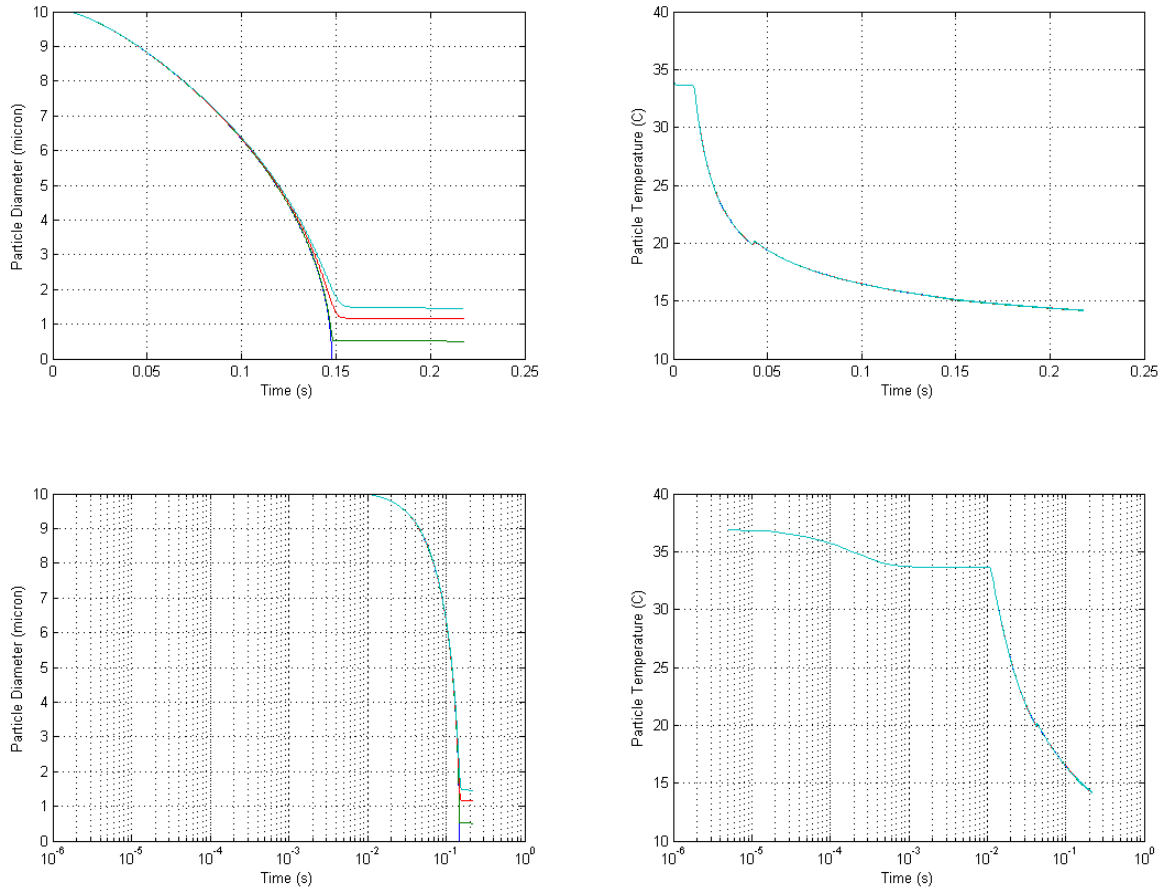

Figure 9: Comparison of pure water droplet diameter and temperature change over time to droplets with initial salinity of 1, 10, and 20%.

In order to validate our model's predictions, we compared our results for binary solution droplets to experimental data from various literature sources. From his studies of hygroscopic aerosols, Tang (1996) developed a polynomial expression to determine the water activity of a sodium chloride solution by simply knowing the mass fraction of the salt. We compare our predicted salt mass fractions at the same humidity (after reaching equilibrium) to the results from this polynomial in Figure 9. For the BSA + water droplet, we calculated the growth factor from the data provided by Mikhailov et al (2004) for both his volume additivity model prediction and the experiments, and then calculated our own growth factor with and without a modification to the Φ term (in equation 3.10) to account for the deliquescence/efflorescence transition. The comparison of these growth factors is shown in Figure 10. Experimental data for the water activity versus mass fraction of solute for a binary aqueous solution droplet of glucose was obtained from Peng et al. (2000). Our model's predictions for a glucose solution droplet are compared with this data in Figure 11.

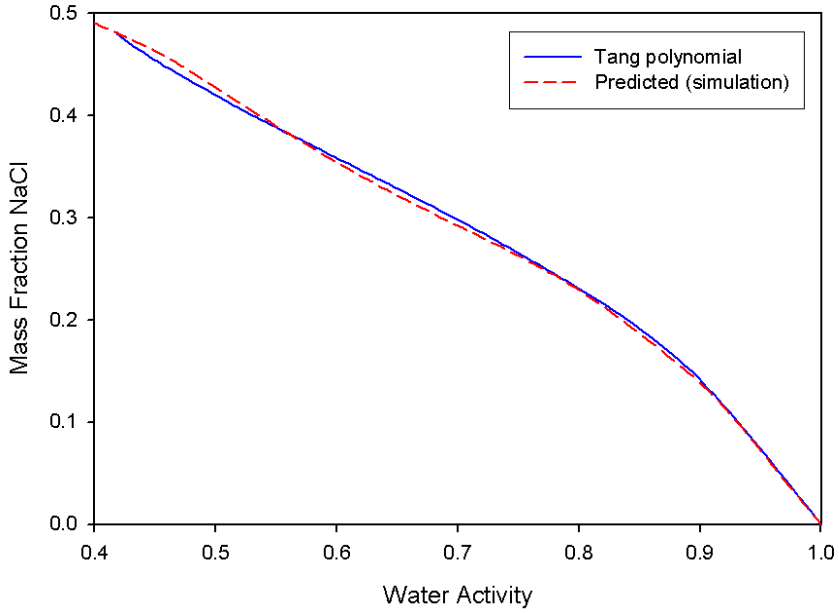

Figure 10: Mass fraction of sodium chloride in binary aqueous solution droplet vs. water activity prediction compared to Tang (1996) polynomial.

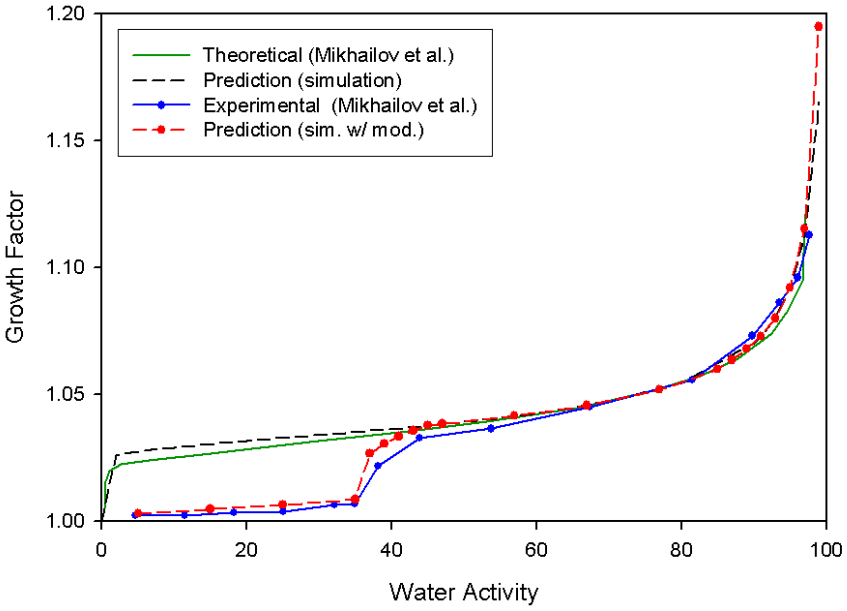

Figure 11: Binary BSA aqueous solution droplet growth factor (D/D_{dry}) vs. water activity predictions compared to the work of Mikhailov et al. (2004).

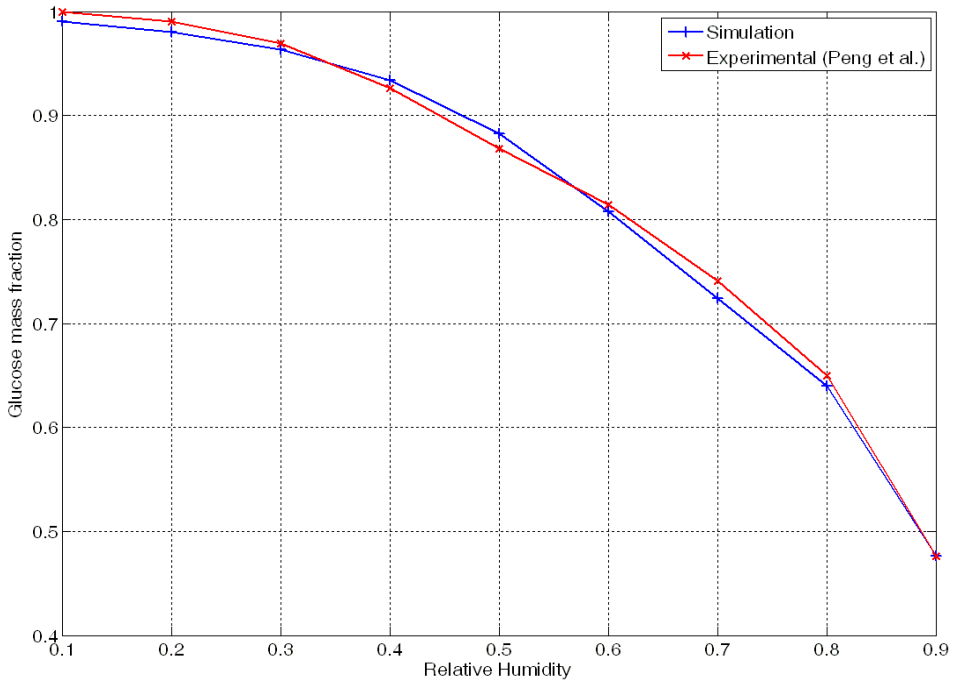

Figure 12: Equilibrium mass fraction of binary aqueous solution of glucose vs. relative humidity predictions compared to the work of Peng et al. (2000).

While the mass fraction of solute upon reaching equilibrium will always be the same at the same relative humidity (unless there is a hysteresis effect), the temperature of the surroundings has a large effect on how long it will take to reach equilibrium. This is displayed in Figure 12, for a 10µm saline droplet, held at constant relative humidity in 40 °C and 5 °C air until reaching equilibrium. The effect of hysteresis (also know as "path-dependency") on a saline droplet is also included in the model. When the efflorescence and deliquescence points of a system do not occur at the same relative humidity, then one cannot predict the properties of the system when it is between these two points simply by knowing the current relative humidity. The droplet was given an initial salt mass fraction, and the surrounding relative humidity was made to change constantly with time, ranging from below the efflorescence to above the deliquescence point of NaCl. Figure 13 illustrates how the mass fraction of NaCl within the droplet at a given time depends

not only on the instantaneous RH, but also on what the RH was earlier in time. It should be noted here that a classical nucleation model was not incorporated into our model, for reasons of simplicity and practicality. Instead, we change the value of the ν term (in equation 3.10) to make the diameter of the droplet suddenly decrease, effectively causing nucleation. When the solute mass fraction is about 0.9 or higher, we consider it to be a "dry" particle (since this value cannot go to 1.0 for computational reasons). An issue with prompting nucleation in this manner, however, is that the nucleation time predicted by the model seems to be a bit too long. A more tedious, thorough modeling of the nucleation event would be needed to correct this, but is not necessary for our purposes at this time.

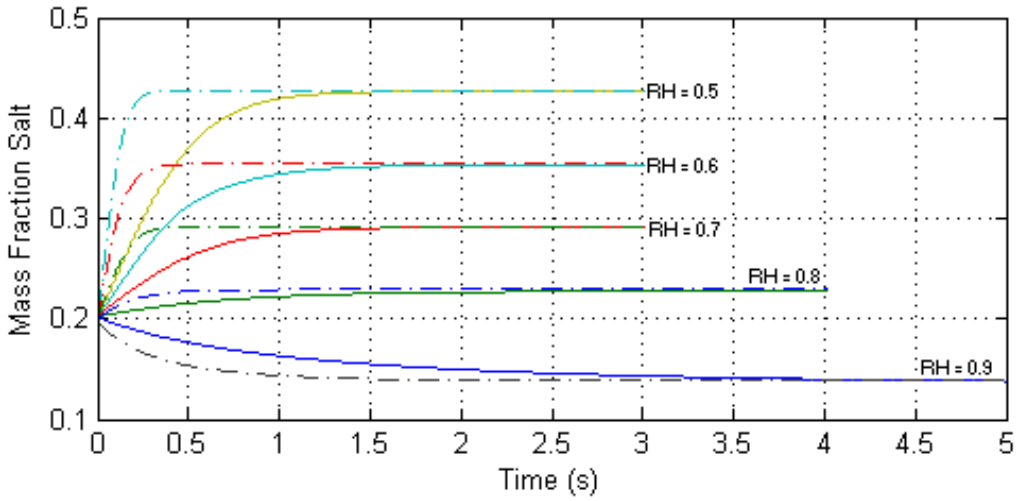

Figure 13: Mass fraction of NaCl in droplet in atmosphere of constant relative humidity vs. time. Dashed lines correspond to an ambient of 40°C, solid lines are for 5°C.

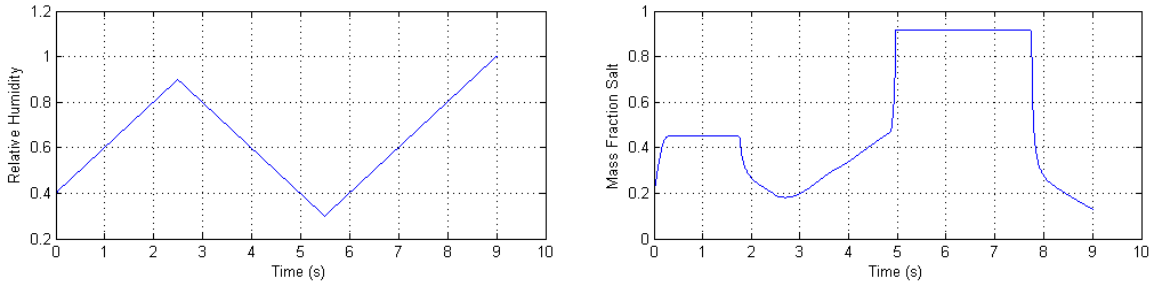

a) b)

Figure 14: The effect of hysteresis on a NaCl binary aqueous solution droplet. a) Change in ambient relative humidity over time. b) NaCl mass fraction over time.

4.5 Multiple Component Droplet

Having proven our model's accuracy for binary aqueous solutions, we next attempted to validate it for ternary solutions. This is a somewhat difficult task due to the scarcity of experimental data on ternary solutions of interest, but the author did manage to find a couple relevant pieces of literature with which to compare our results. Comesaña et al. (2001) found the water activity of glucose + sodium chloride + water systems and plotted the glucose vs. sodium chloride molalities at lines of constant relative humidity. Figure 14 shows our predictions match the data almost perfectly. Unfortunately, however, the range of relative humidity for which experimental data is reported is very limited (85% to 97%). Subsequently, we took the experimental data for BSA + NaCl + water systems, as reported by Mikhailov et al. (2004), and calculated the growth factor. Then we compared this to the growth factor calculated from our model, shown in Figure 15. As can be observed, our model predicts the experimental results fairly well, even for an organic/electrolyte mixture. The slight over-prediction of the model as the ratio of salt mass fraction (xs) to BSA mass fraction (xp) tends to 1.0 can be attributed (mostly) to electric charge effects between the molecules, which are not accounted for in our model.

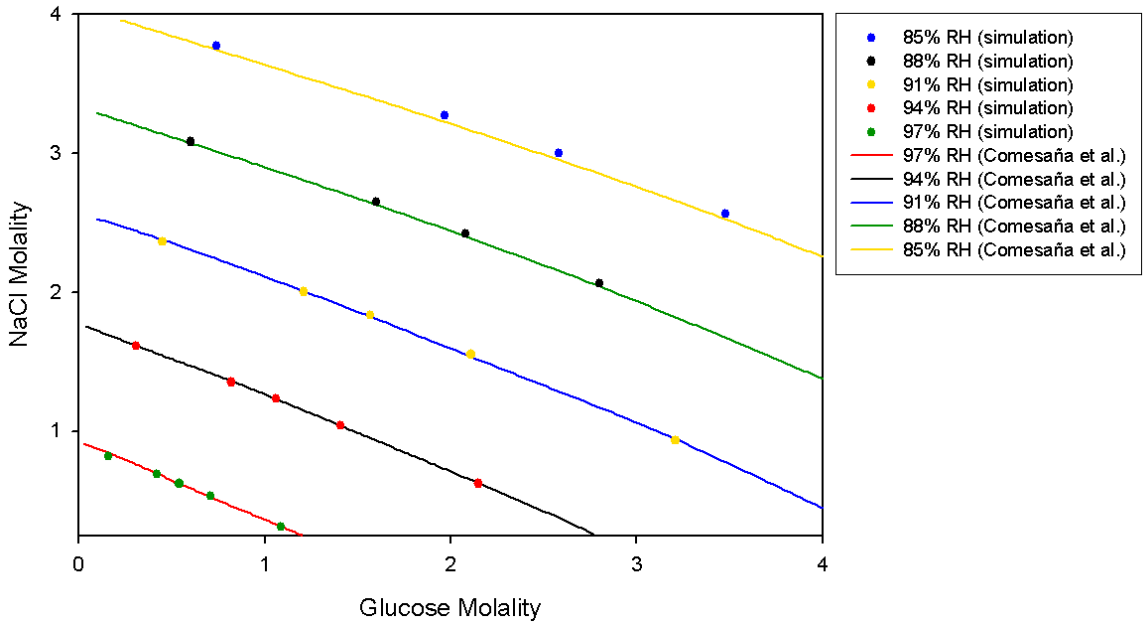

Figure 15: Ternary solution droplet of NaCl + glucose + water predictions compared to the work of Comesaña et al. (2001).

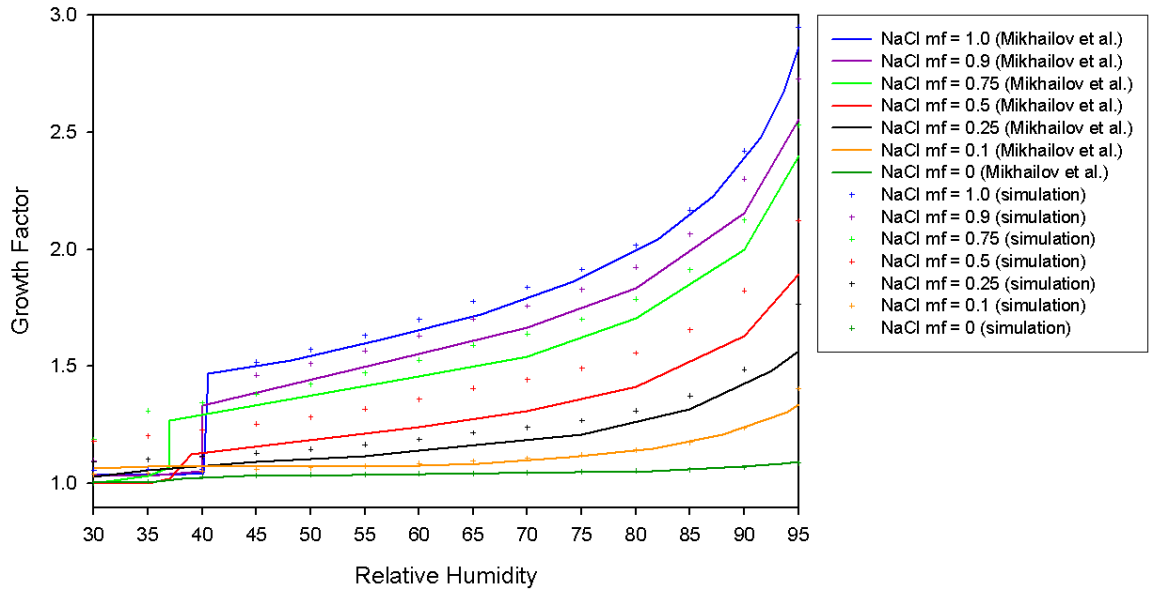

Figure 16: Ternary solution droplet of NaCl + BSA + water growth factor predictions compared to the work of Mikhailov et al. (2004)

In addition to NaCl, BSA, and glucose, the lipid content present in a droplet of sputum can [theoretically] have a significant effect on the evaporation of water from the droplet.

Since we could not find any literature on the effects of adding lipids or DNA to the spraying medium, we have made a couple assumptions for these two constituents. First, we assume that the lipids will increase the stability of the virus, because the viral envelope is partially composed of lipids. Another reason is that lipids are amphiphilic, which means that lipid molecules may "migrate" to the air-water (or air-droplet) interface and form a monolayer, and thus retard the evaporation process. As for the DNA content, due to lack of specific data and the fact that its relative concentration within the sputum is very low, we assume that it has no effect on the infectivity of the virus, and we only take into account its molecular weight in our calculations. In Figure 17, below, we compare our model's predictions for a pure water droplet, denoted by blue line, a saline droplet, depicted by green line, a sputum droplet (containing all of the constituents in the concentrations listed for purulent sputum in Table 2.1), represented by yellow line, and a sputum droplet with a 50% reduction in evaporation rate (due to the lipids forming a monolayer, as discussed in Chapter 2), denoted by red line. Note that the red line obscures all of the other lines in the temperature plot, since all droplets are held at the same conditions and thus reach the same wet bulb temperature. Though the length of time required for each droplet to reach this temperature will be slightly different, the time scale for this event is miniscule compared to the total time shown (12 seconds).

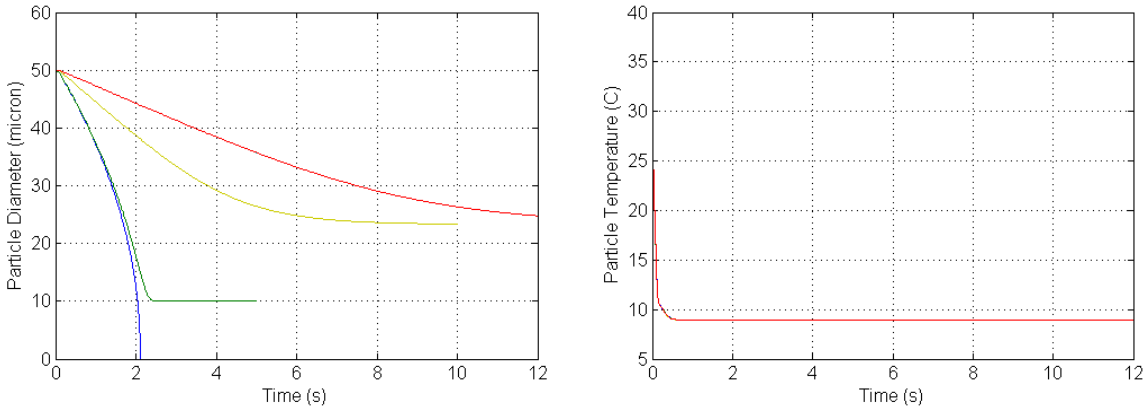

Figure 17: Diameter and temperature change over time of droplets of different composition under the same conditions.

4.6 FLUENT Evaporating Droplet Comparison

In order to help validate the results obtained from our in-house code, as well as to explore the practicality of simulating droplet evaporation in FLUENT, a case was set up with a single droplet of pure water injected into a jet of air that is emanating into a room of stagnant air. To begin with, a flow field was needed, so a mesh was made in GAMBIT. To keep things simple, a rectangular "room" was created, measuring 1x1x3 m, with a single inlet in the center of one wall, and a single outlet at the opposite end of the room on the ceiling. The inlet had a diameter of 0.01905 m and was set as a "velocity inlet", and the outlet was given a diameter of 0.09525 m and set as a "pressure outlet". These values correspond to the inlet pipe and a damper of the experimental chamber. The geometry was then meshed using a triangular paved mesh and a tetrahedral scheme for the volume, with about 180,000 nodes all together. The grid of the room can be seen below in Figure 17.

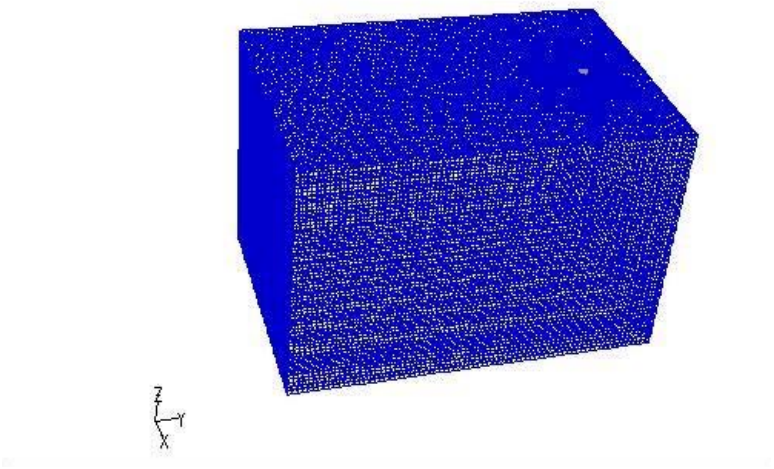

Figure 18: Grid for single droplet evaporation case in FLUENT.

Next, the case had to be set up in FLUENT. The unsteady implicit solver was used with the realizable k-ε turbulence model. This model was chosen because FLUENT recommends it for more accurate prediction of the spreading rate of round jets (FLUENT, 2001). Then temperature and species transport were enabled in the calculations, with the default "mixture-template" (consisting of H2O, O2, and N2) as the mixture. An injection was set with a single droplet entering from the center of the inlet at the very beginning of the simulation, with a diameter of 10 μm and a temperature of 310 K. The operating temperature and outlet boundary temperature were both set at 294 °K, and the species concentration of O2 at both the inlet and outlet were changed to 0.22 (corresponding to the mass percentage of oxygen in air). Finally, the time step was set at 1e-03 seconds, and iterations were run until about 3e-03 seconds after the droplet had completely evaporated. Such things as relative humidity of the inlet or ambient air, or salts or other solids contained within the droplet, were not considered in this case for the sake of time and simplicity.

From the results depicted below (in Figures 18-20), FLUENT appears to match our predictions quite well. While the mass from the two simulations is quite close, the diameter tends away from the MATLAB prediction with time, and the temperature plot does not show the sharp drop from the initial temperature. The diameter discrepancy as time goes beyond 4e-02 seconds can be attributed to the use of a fixed time step in FLUENT. The two lines would most likely match if the time step decreased beyond this point. The same can be said of the droplet temperature, only for the beginning of the simulation instead of the end, since it can be seen from the MATLAB data that the temperature drops from the initial temperature to the wet bulb temperature in a very short time. Also, refining the mesh should help with the accuracy (as the mesh used in this simulation was fairly course in some areas).

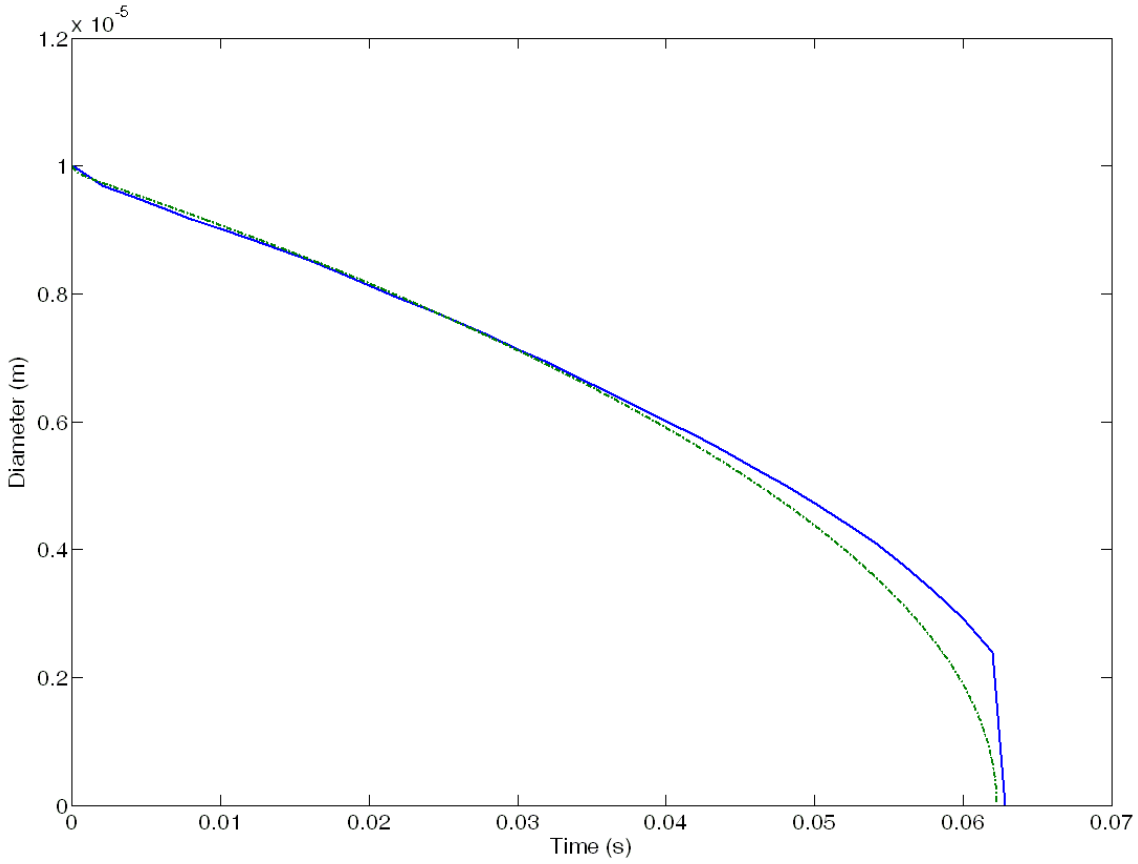

Figure 19: Comparison of droplet diameter change with time between the FLUENT (solid blue) simulation and the in-house code (dashed green).

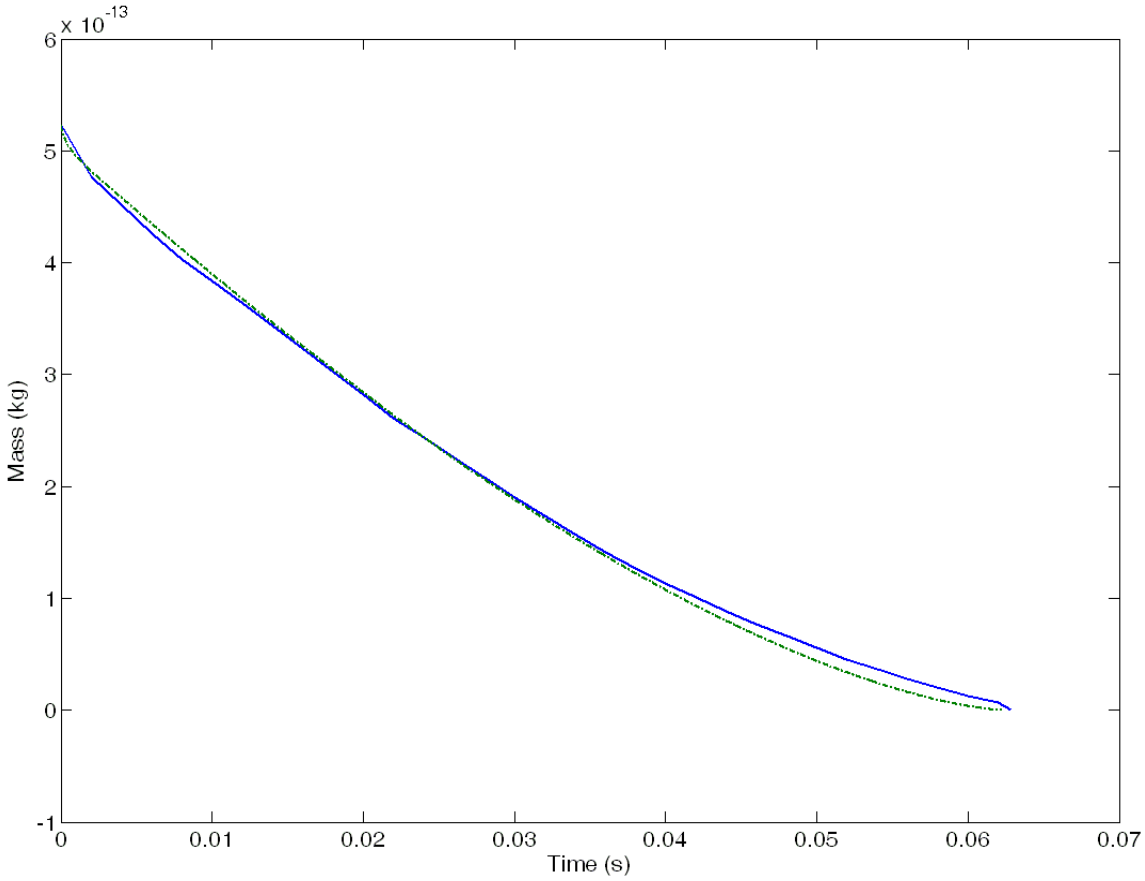

Figure 20: Comparison of droplet mass change with time between the FLUENT (solid blue) simulation and the in-house code (dashed green).

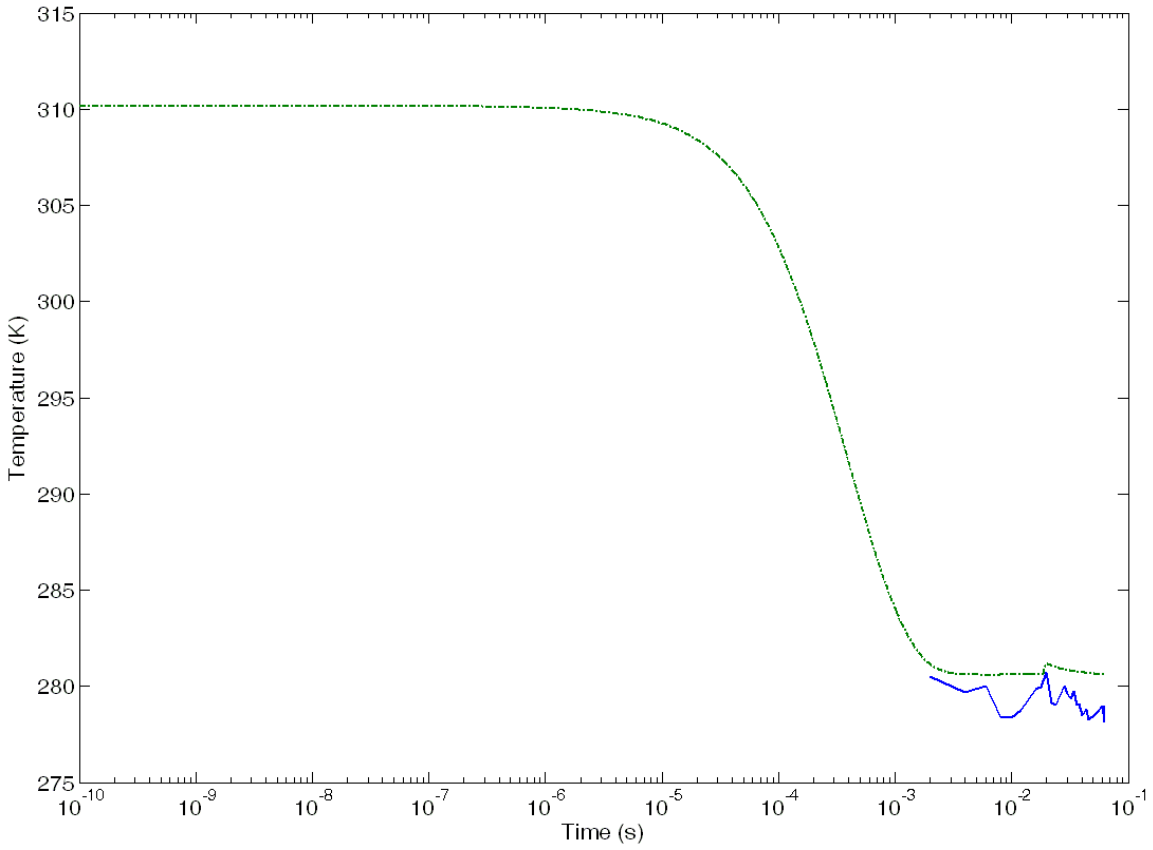

Figure 21: Comparison of droplet temperature change with time between the FLUENT (solid blue) simulation and the in-house code (dashed green).

4.7 Droplet in Field of Homogeneous Turbulence

In order to simulate the behavior of a droplet placed into air with only small turbulent fluctuations in the velocity (i.e. no average velocity), we borrowed from WVU's Random Flow Generator (RFG) code (Smirnov et al., 2001). The function for the air velocity calculation was changed from a buoyant jet to a modified RFG function, where the velocity calculation depends on the time step and the prescribed turbulent length scale. An example of a single droplet's trajectory in 3-dimensional space is shown in Figure 21.

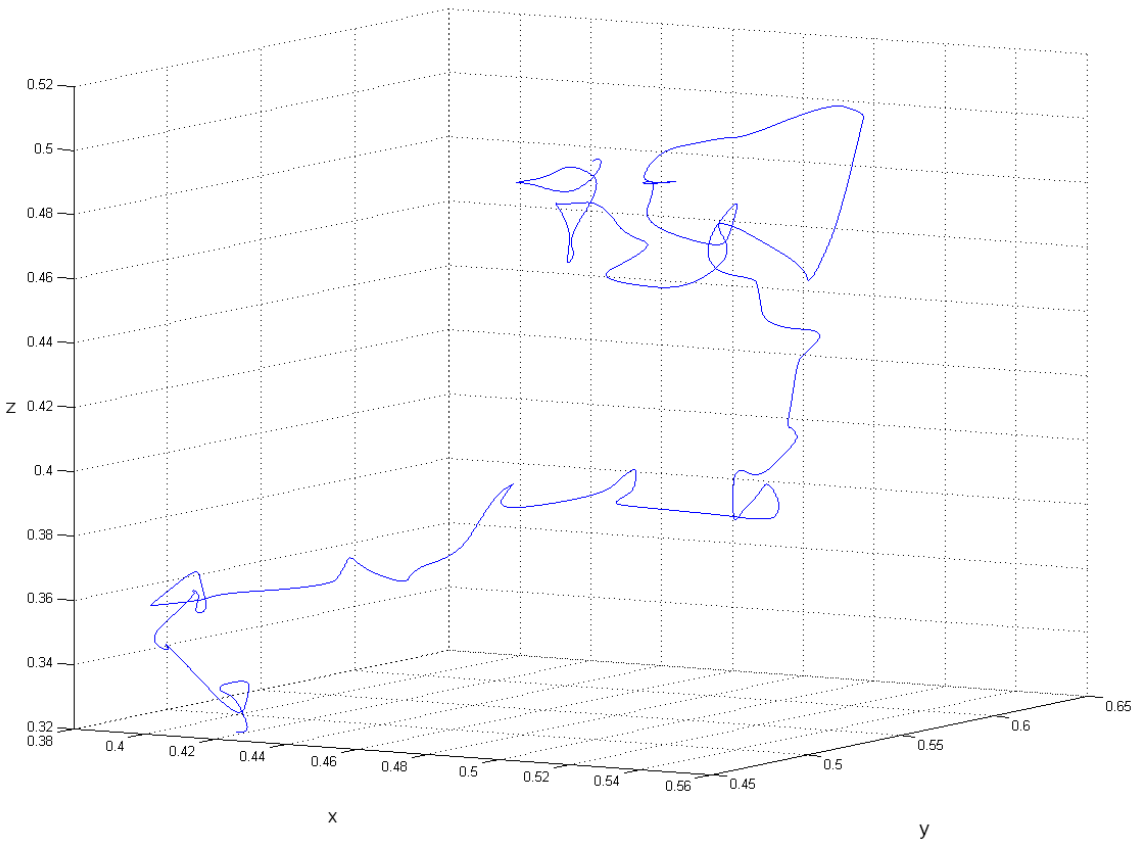

Figure 22: Three dimensional trajectory of a droplet following turbulent fluctuations in the surroundings.

Chapter 5: Coughed Particle Dispersion in Experimental Chamber

5.1 Introduction

West Virginia University and NIOSH have been working very closely on a study of the spread of airborne influenza virus, in an effort to develop effective measures for infection and pandemic prevention. NIOSH has set up an "experimental chamber" at their Morgantown facility to study the spread of particles produced by a human cough. For this purpose, they have developed a "cough machine" (Figure 22, below), which is capable of producing the same flow vs. time profile and particle size distribution as an average human cough would have, effectively reproducing an "real" human cough. Through the use of the commercial CFD code FLUENT, we have simulated a mannequin coughing in this chamber, as well as the actual cough machine emitting a "cough" inside of the chamber, in order to try to predict where the particles from the cough will travel within a room.

Figure 23: The cough machine in the experimental room at NIOSH. Image courtesy of Dr. W.G. Lindsley, NIOSH.

5.2 Geometries and Grids

All three of the grids created for the FLUENT simulations were made with the grid-generation software GAMBIT. The first grid created for the experimental chamber simulations had a simple "mannequin" standing in one corner, with its back to the wall, facing into the room. Opposite the mannequin, on the ceiling, there was a small damper (outlet). The dimensions of the experimental chamber are 2.7432 x 2.7432 x 2.3876 m (LxWxH). The diameter of the mouth of the mannequin was 0.01905 m and the damper (seen as a small circle at the back of the room, on the ceiling) had a diameter of 0.09525

m. The mesh of the room had a total of 554,028 tetrahedral cells. The grid (with two of the walls removed in order to better display the mannequin) is shown below in Figure 23.

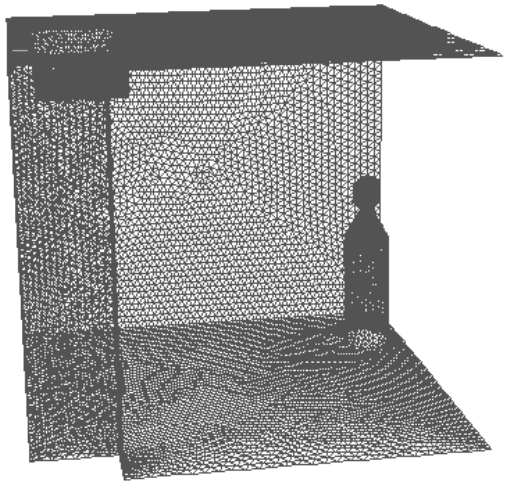

Figure 24: Mesh of room with mannequin standing in corner.

The second grid for the experimental chamber saw the removal of the mannequin and the creation of a relatively detailed and accurately scaled cough machine, depicted in Figure 24, below.

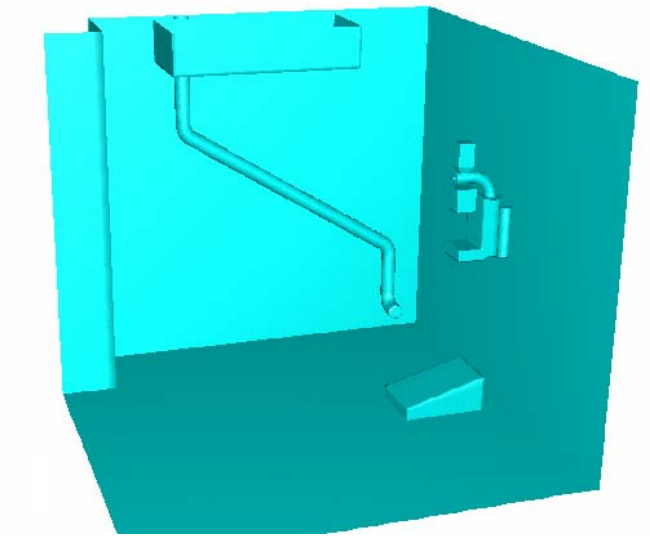

Figure 25: Original setup of cough machine in experimental chamber.

Figures 25 and 26 show close-up comparisons between the actual machine used in the experiments and the simplified one created for the simulations. Figure 26 also includes an example of the mesh on the machine.

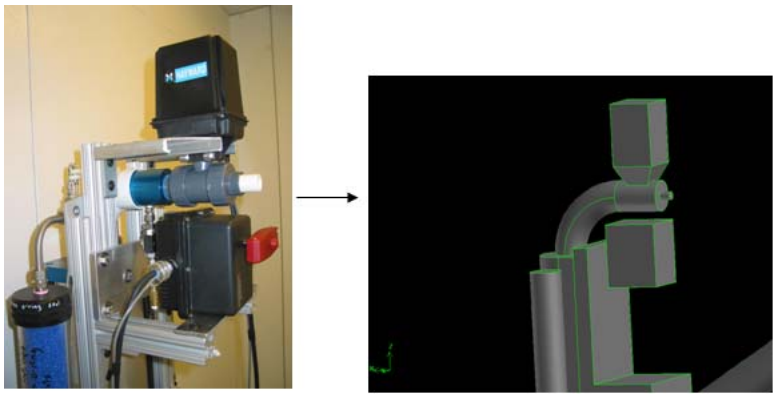

Figure 26: Actual cough machine compared with the simplified geometry generated in GAMBIT.

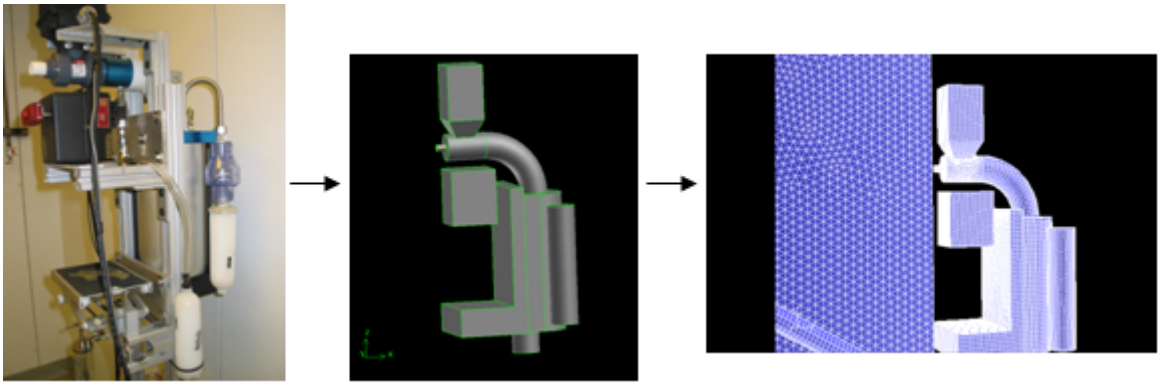

Figure 27: Actual cough machine compared with the simplified geometry and mesh generated in GAMBIT.

The third, and final, geometry of the chamber is a simplified version of the second, with all unnecessary details removed for better computational efficiency, and the cough machine moved to the opposite side of the room (it was switched for experimental reasons), and is shown in Figure 27.

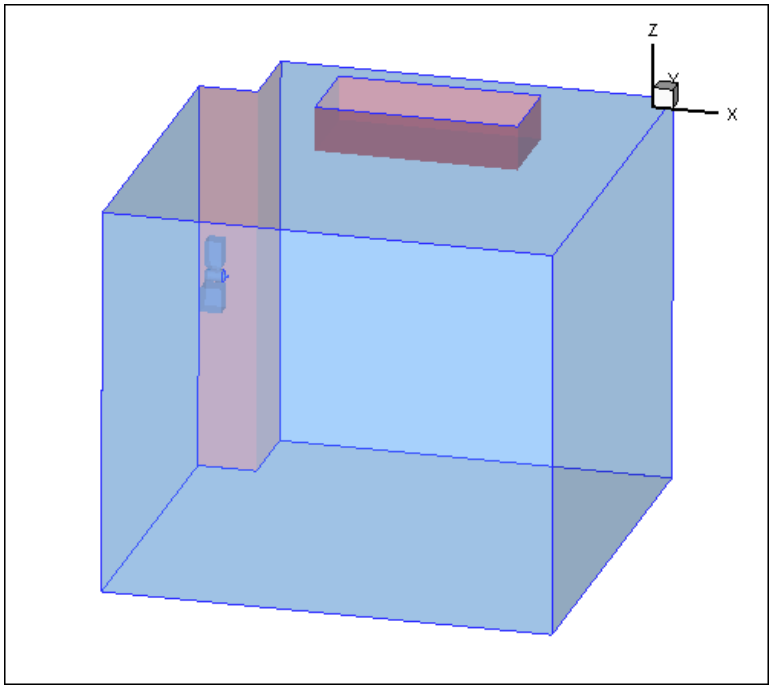

Figure 28: Experimental chamber with cough machine revised geometry.

5.3 Boundary and Injection Conditions

The first case (with the mannequin) was simulated in FLUENT using the k-epsilon RNG turbulence model, since it is a well known and oft-used model that can predict turbulent behavior with reasonable accuracy while remaining computationally efficient. A transient inlet velocity was given at the mouth, using experimental cough flow rate data provided by NIOSH, shown in Figure 28. The first cough is at 100% flow rate, followed by a second cough at 70% flow rate, and a third at 50%. The damper was set as a pressure outlet with zero gauge pressure. The temperature of the inlet and ambient were set at 310.15 and 294.15 K, respectively (corresponding to human body temperature and normal room temperature). A surface injection of 1 micron, inert, mass-less particles was then specified at the inlet so that the particles would follow the flow. The particles were

injected at every fluid time step (72 particles every 0.005 seconds), for a total of 10,800 particles per cough. In this and in all of the following cases, the velocity of the air coming from the inlet was specified to be uniform across the face or boundary of the inlet, implying the assumption of a smooth contraction nozzle (rather than a long pipe) for the inlet.

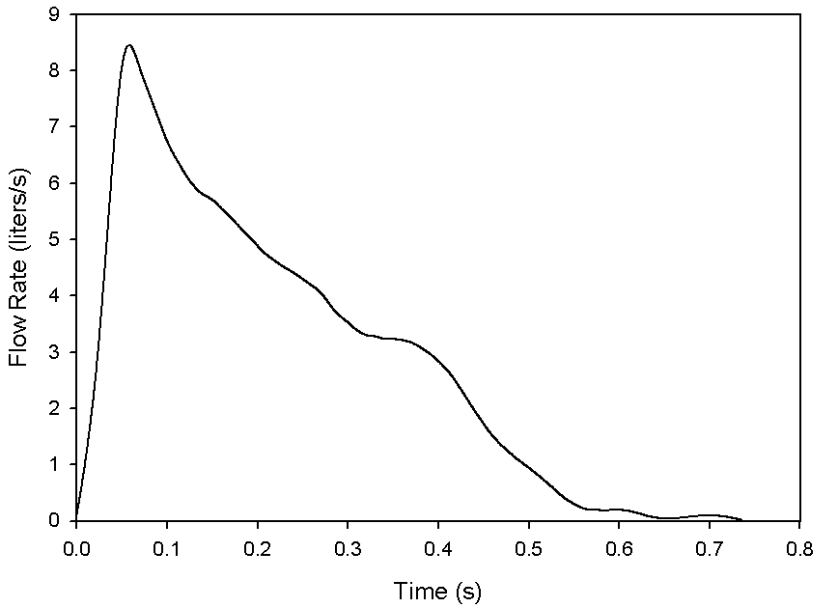

Figure 29: Simulated cough flow rate (data provided by NIOSH).

The second case (with the cough machine on the right) was also simulated with the k-epsilon turbulence model, and had the same transient inlet velocity prescribed at the "mouth" as in the previous case, as well as the same flow time step. In this case, all of the walls of the room were set as pressure outlets with zero gauge pressure, and everything was assumed to be isothermal (the temperature equation was not activated in the calculations). Instead of a particle injection, this time a scalar was introduced with

inlet diffusion, as an alternative method of visualizing the spread of three coughs within the chamber. The scalar was given a value of 1, and a constant diffusivity of 100.

The third case (with the cough machine on the left) was simulated using the realizable k-epsilon turbulence model, with the same inlet conditions as the second case, however with only one cough having a flow rate the same as in Figure 28. For this case, just the back-corner wall and the "box" on the ceiling were set as pressure outlets, shown in red in Figure 27, and the temperature was again neglected. The purpose of this simulation being to attempt to match the dispersion of particles as measured in experiments, a surface injection (for uniformity over the surface of the inlet) of inert 0.4 μm particles was created. This size diameter was chosen because it represents the largest amount of particles in the experiments for which the data reported by the particle counters is considered to be reliably accurate. The density of the particles was specified to be 1,987 kg/m^3, which is the density of potassium chloride (the material used for the particles generated in the experiments). Particles were injected over the duration of the cough (0.75 seconds), with a particle time step of 2.5×10^{-4} seconds, whereas the time step for the continuous phase was the same as in the two previous cases. The smaller time step for the particles not only increases the accuracy, it increases the total number of particles injected during the cough, as well. In order to have the particles injected at each particle time step (rather than at the fluid time step), the option for two-way coupling of the discrete phase had to be enabled in FLUENT. This means that not only will the continuous phase affect the particles, but the effect of the particles on the continuous phase is also taken into account. This option was then turned off after 1 second, since the

injection was complete and the particles had spread out somewhat by this time and it could be assumed that the particle volume fraction was low enough that the effect of the particles on the continuous phase was negligible. Ideally, this option would be kept on for the entire simulation, however it was found to have a significant detrimental effect on the speed of the computations, and was not necessary for our particular case. There were 459,000 particles in total injected in this case.

For the fourth case, as an alternative to injecting particles and attempting to compare the amounts captured, a scalar was again introduced, this time with the intent of comparing the trend of scalar concentration at each spectrometer location to the experimental data. The settings for this case were the same as the previous, but without an injection of particles, of course. The value of the scalar was defined as 1 at the inlet for the duration of the cough, and 0 thereafter. A user-defined function (UDF) was used to calculate the scalar diffusivity by dividing the turbulent viscosity (calculated by FLUENT) by the Schmidt number (constant, set at 0.7).

5.4 Multiple Cough Simulation Results

It has been observed through common experience that when a person with an upper-respiratory infection coughs, often-times it is not just a single cough, but multiple, consecutive coughs. For this reason we decided to simulate three consecutive coughs coming from the mouth of the mannequin inside of the experimental chamber, with the boundary conditions as specified in the previous section. The plot of velocity vs. time at

the inlet for this simulation is presented in Figure 29, below. Images of the grid with the particles colored by residence time at the end of each cough are displayed in Figures 30-32. These images give an idea of how infectious particles disseminate in the air upon leaving the mouth of a coughing individual.

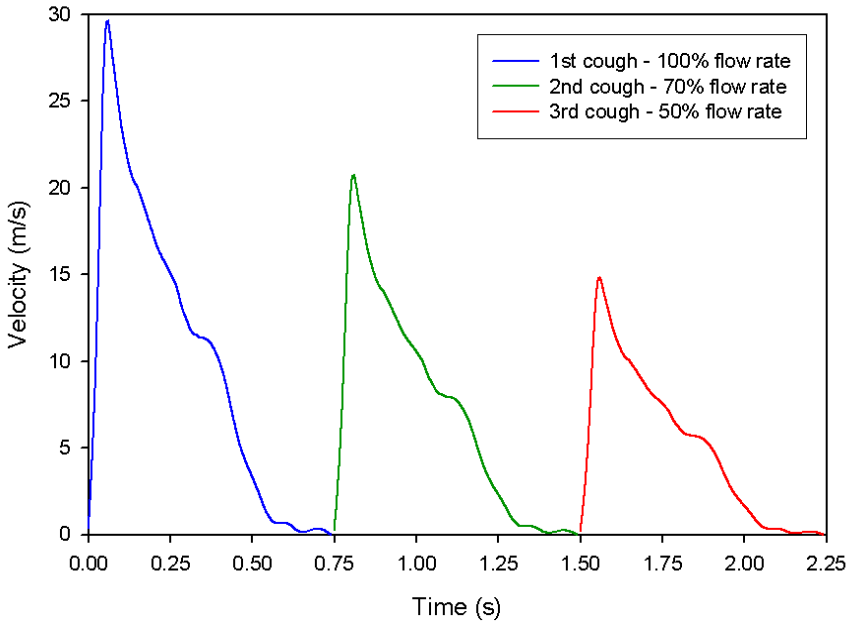

Figure 30: Transient cough velocity prescribed at inlet (mouth of mannequin) for case of three consecutive, diminishing coughs.

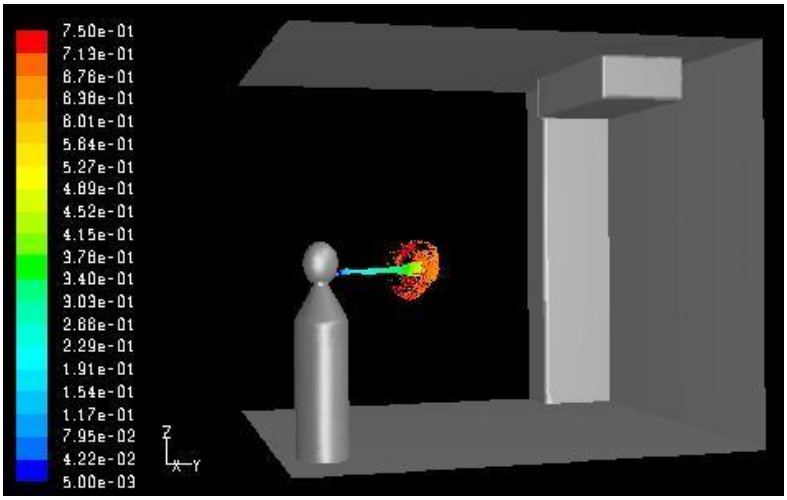

Figure 31: Particles colored by residence time at 0.75 seconds (end of first cough).

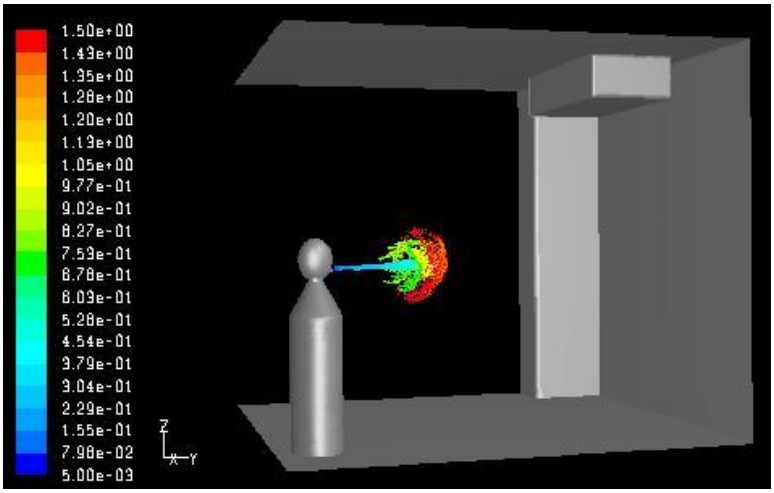

Figure 32: Particles colored by residence time at 1.5 seconds (end of second cough).

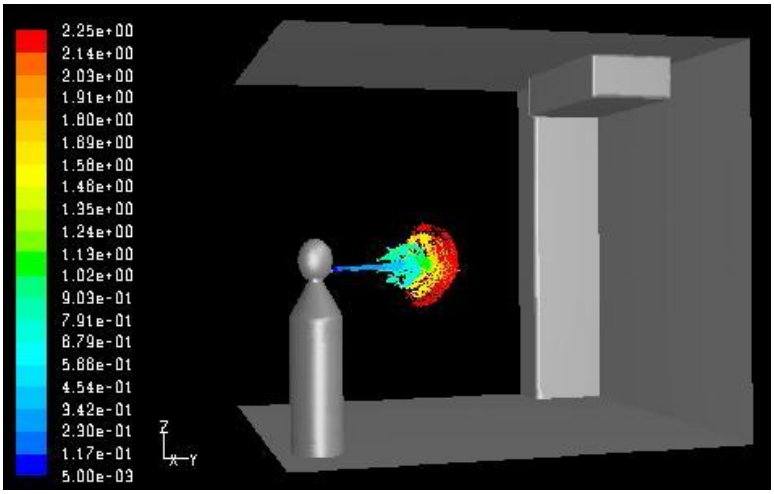

Figure 33: Particles colored by residence time at 2.25 seconds (end of third cough).

Figures 33 through 36 depict the results obtained from the second case, which utilized a user-defined scalar rather than a particle injection. In only four seconds, the scalar "cloud" is shown to have almost reached the opposite side of the room, a distance of over 2 meters from its origin. It also appears to have almost completely diffused in the region from the mouth to about 1 meter away by this time.

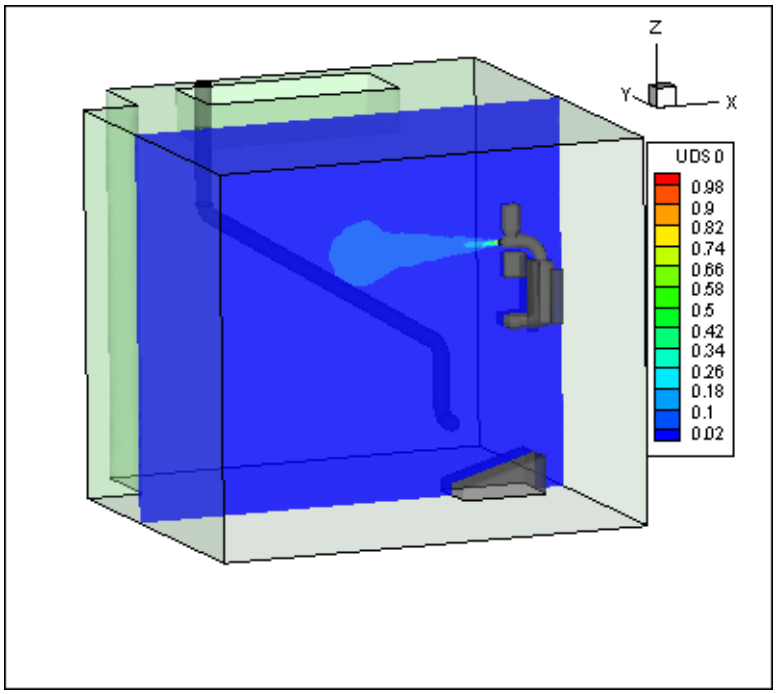

Figure 34: Vertical contour slice through the center of the inlet colored by scalar concentration at 0.75 seconds (end of first cough).

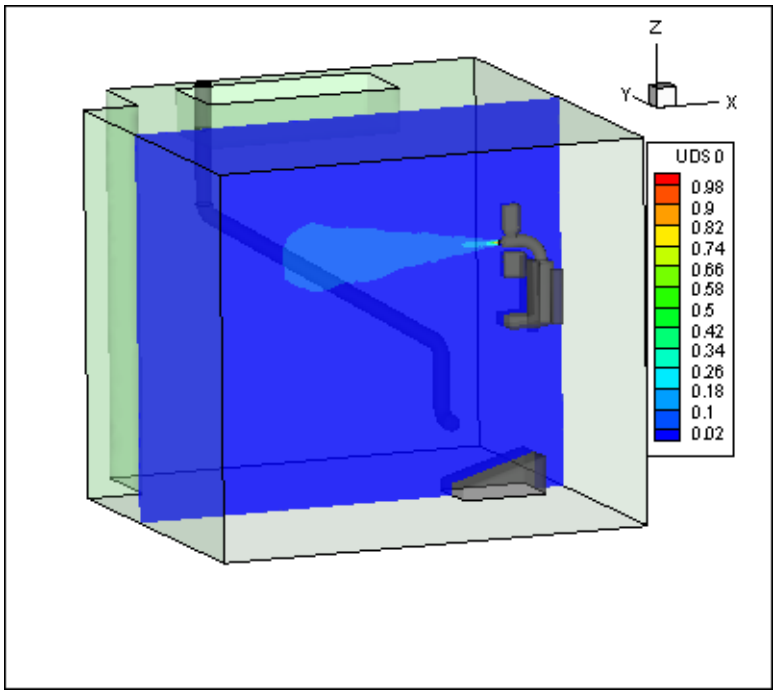

Figure 35: Vertical contour slice through the center of the inlet colored by scalar concentration at 1.5 seconds (end of second cough).

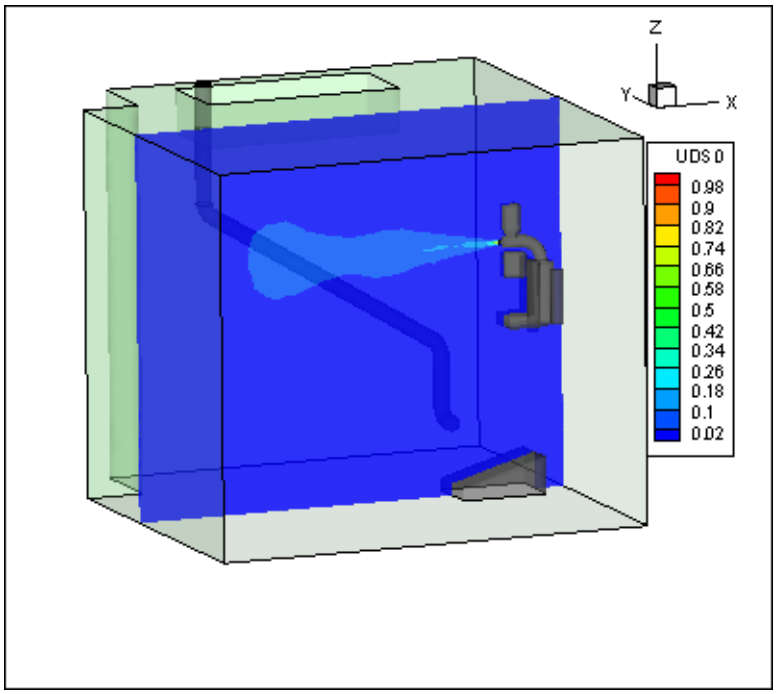

Figure 36: Vertical contour slice through the center of the inlet colored by scalar concentration at 2.25 seconds (end of third cough).

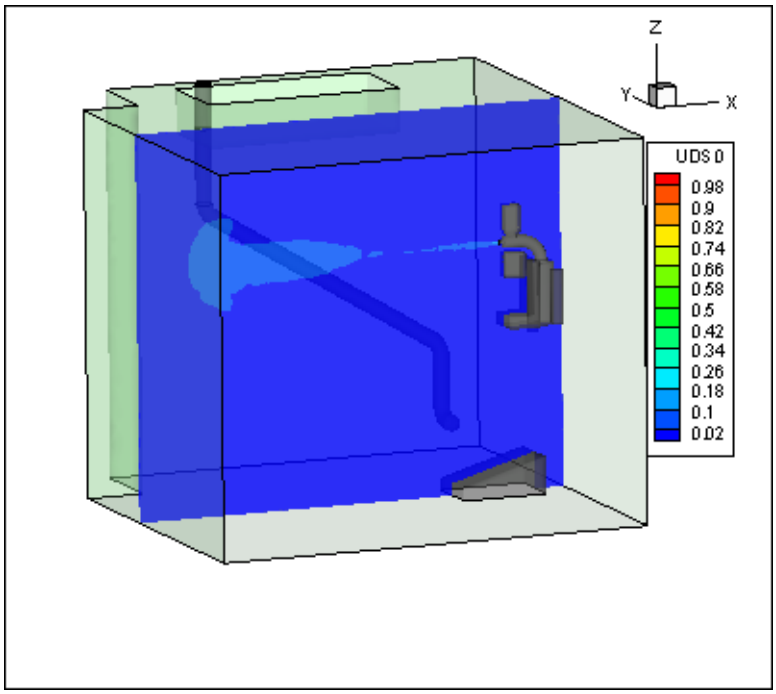

Figure 37: Vertical contour slice through the center of the inlet colored by scalar concentration at 4 seconds (1.75 seconds after end of third cough).

5.5 Single Cough Simulation and Particle Dispersion

The cough simulator at the NIOSH facility was set up to produce dry particles of potassium chloride of approximately the same size distribution as measured experimentally from a human cough, in order to be able to reproduce the conditions of a "real" cough in a controlled environment. The particles within the cylinder of the machine (i.e. the particles to be "coughed out") are counted by an aerodynamic particle sizer prior to the cough, then the air (and particles) inside of the cylinder is forced out by a piston with the same flow rate as a human cough. There are five Grimm 1.108 aerosol spectrometers placed at specific locations inside of the experimental chamber, in two different configurations, as shown in Figures 37 and 38. The first two experiments were done with the first configuration (Fig. 37) and the last three experiments with the second configuration (Fig. 38). The ambient conditions within the chamber were roughly the same from one experiment to the next, with the temperature between 19-26 °C, the pressure between 975-984 mb, and relative humidity between 30-59%, which is below the deliquescence point of potassium chloride (so the particles should remain dry and therefore stay the same size and mass from birth to capture). The experimental chamber is claimed to be air-tight, with no airflow in the room prior to the cough—there is no specified inlet or outlet for the chamber. The spectrometers take in air at a rate of 1.2 liters/minute, and report the amounts of each size (diameter) particle captured over 6-second intervals. In order to compare the data obtained from the experiments to the results of the FLUENT simulations, averages for experiments 1 & 2 and for experiments 3, 4, & 5 needed to be determined. Due to the 6 second spectrometer reporting interval,

and the de-synchronization between the different spectrometers (with respect to the cough initialization), a determination of the amount of particles captured per second by each spectrometer (in each experiment) was deemed necessary for the averaging of experiments. The particle count per second for each spectrometer was estimated by finding the mean of the amount reported at every 6 second interval, and these values were subsequently averaged together for the experiments performed under each of the two configurations. The average particle count per total (for 0.4 μm diameter particles) in cough for each spectrometer (for each configuration) versus time after cough initialization is plotted in Figures 39 and 40. The average background noise in the experiments was determined to be an order of magnitude smaller than the lowest experimental counts, so a correction to the data due to noise was thus deemed unnecessary. Due to the computational expense and resources needed to obtain this much real-time data from a simulation, only the first 60 seconds after the cough are utilized for comparison.

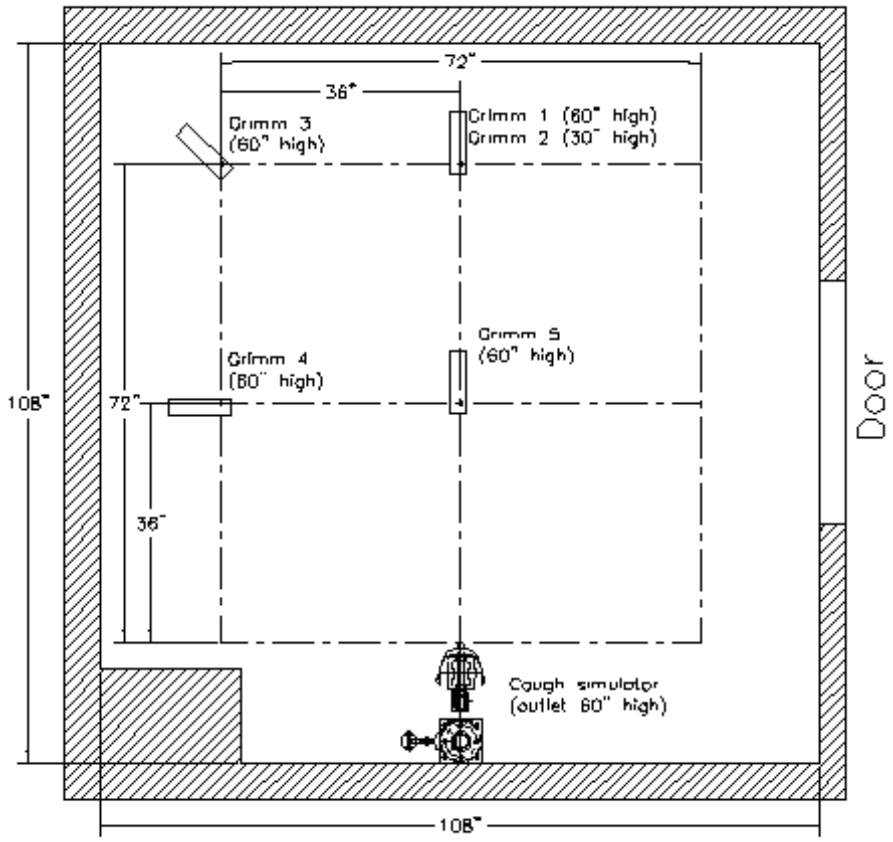

Figure 38: NIOSH experimental chamber Grimm (particle counter) placement for the first two experiments. Image courtesy of Dr. W.G. Lindsley, NIOSH.

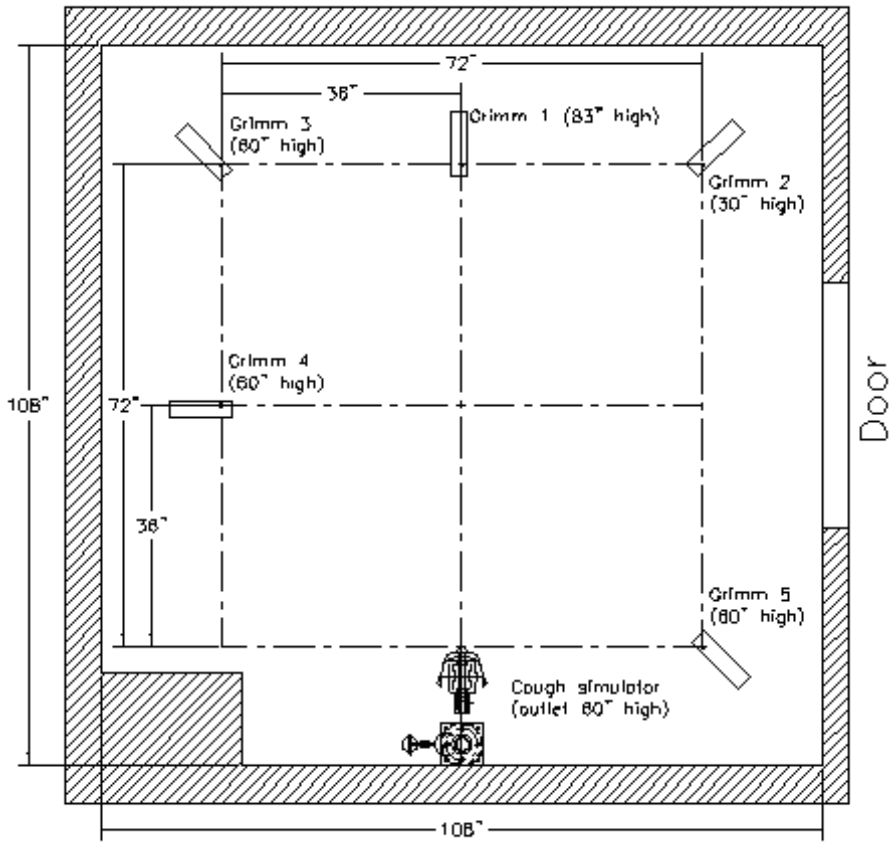

Figure 39: NIOSH experimental chamber Grimm (particle counter) placement for last three experiments. Image courtesy of Dr. W.G. Lindsley, NIOSH.

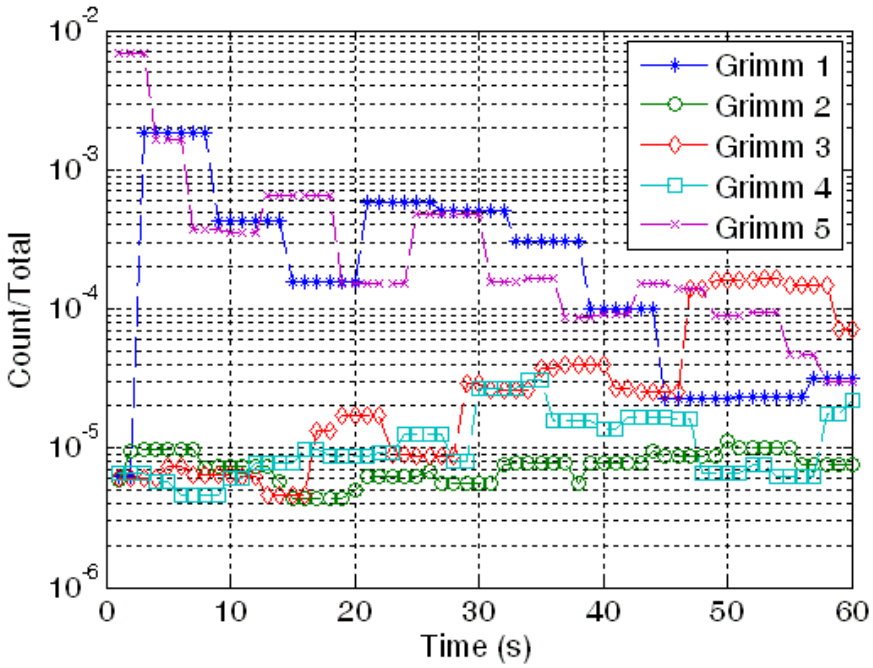

Figure 40: Experimental averages of particle count fractions for each spectrometer for setup #1 (experiments 1 & 2).

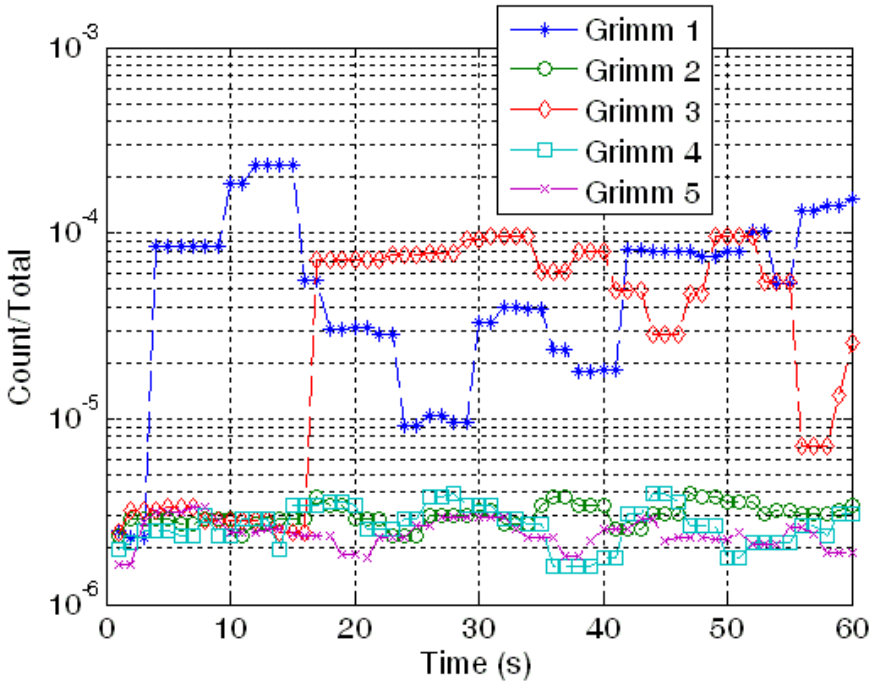

Figure 41: Experimental averages of particle count fractions for each spectrometer for setup #2 (experiments 3, 4 & 5).

In order to obtain the number of particles captured per second at each of the spectrometer locations in the simulations, the FLUENT particle data at each second was first written to a file. A code was then written in MATLAB which reads each file and "traps" the particles that are within a specified x, y, and z distance from each spectrometer location. This effectively puts the spectrometers into the simulation domain. The reason for not creating the spectrometers when originally designing the grid is, again, computational expense and resources. The size of a spectrometer is very small compared to the size of the entire chamber, so the mesh around each spectrometer would have to be much finer than it is without them, ultimately resulting in a much higher cell count for the mesh of the room volume. This would greatly increase the time it takes to run the simulations. After obtaining the number of particles trapped at each location, these amounts were then divided by the total amount of particles that were injected in the domain so that the results of the simulation could be compared with the experiments. Figures 41 and 42 show the comparison between simulation and experiment for the first and second spectrometer setups, respectively, with the inclusion of standard deviation error bars for the experimental averages. No particles were captured at locations 2, 3, and 4 for the first setup in the simulation over 60 seconds, hence the blue line is not present in those plots. The blue line is also not present for locations 4 and 5 of the second setup for the same reason.

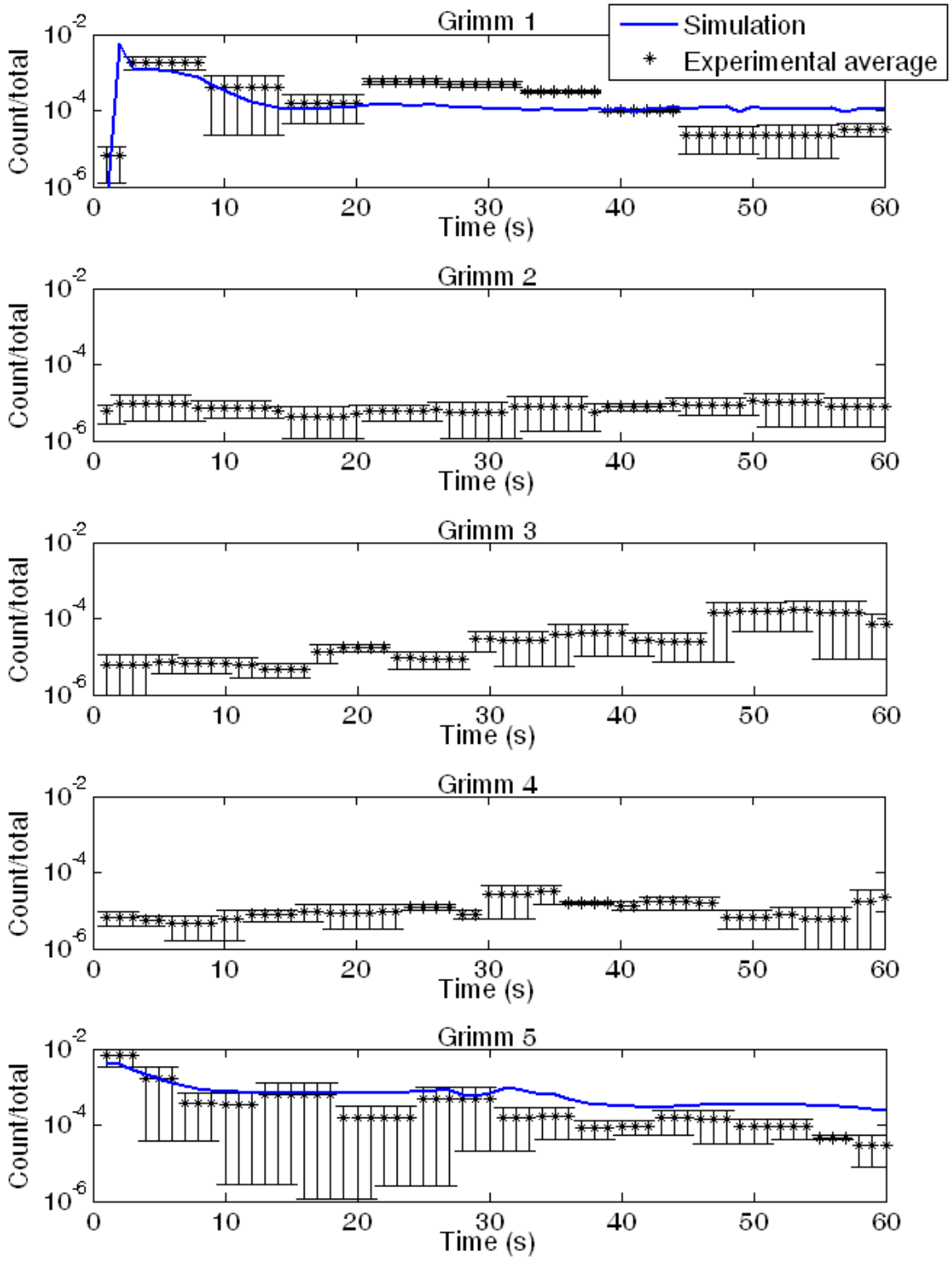

Figure 42: Simulation to experimental data comparison of particles collected at each Grimm spectrometer location in setup #1.

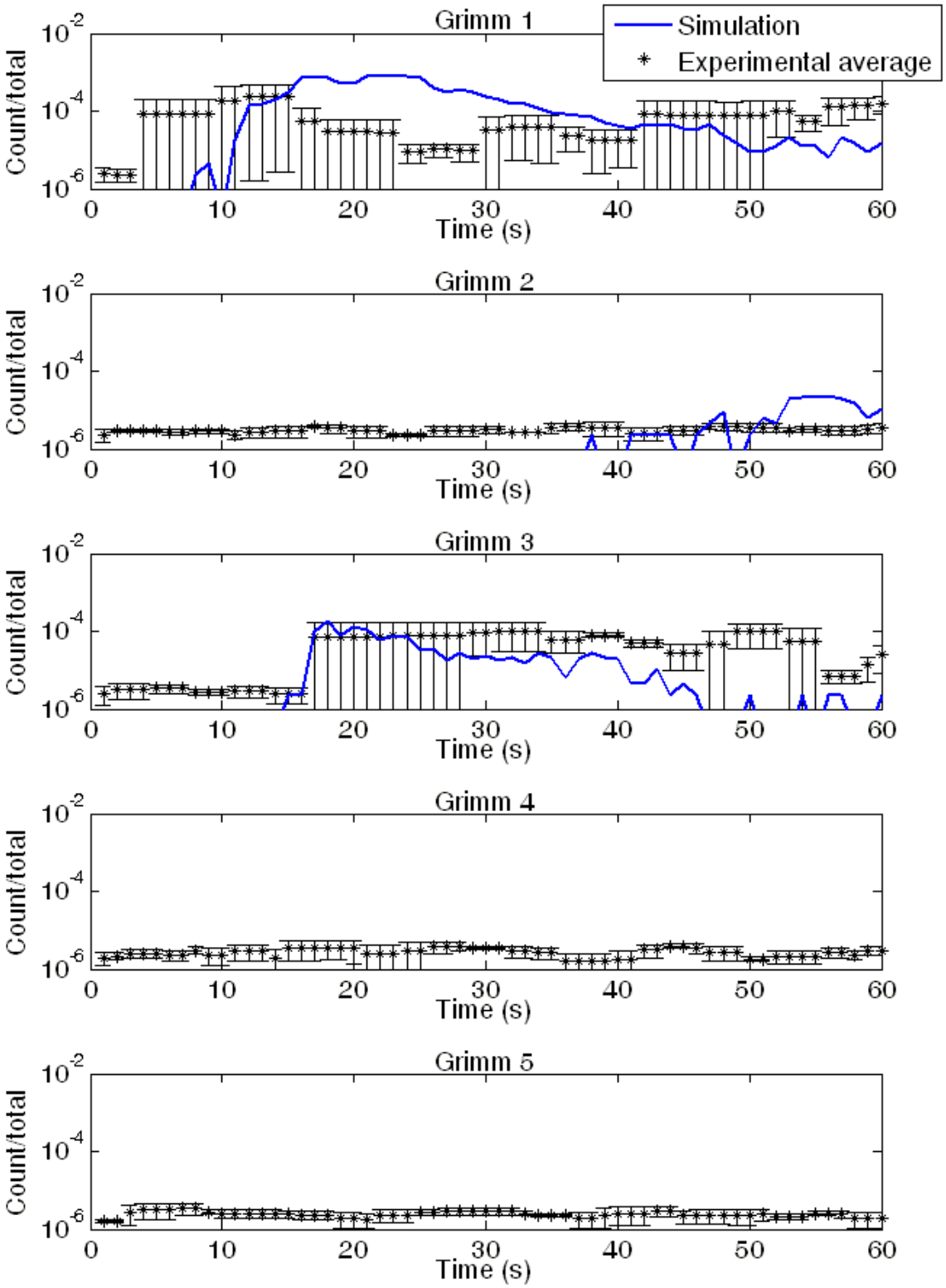

Figure 43: Simulation to experimental data comparison of particles collected at each Grimm spectrometer location in setup #2.

In order to compare the scalar concentrations and experimental particle data, both had to be scaled by a relevant normalization factor. For the scalar concentration data, that factor was taken to be the value of the scalar at the location of Grimm #3 at 60 seconds. For the experimental data, the normalization factor was taken as the average of the values at the third Grimm over the entire 60 seconds. All of the scalar concentrations and the experimental counts at each location were then divided by their respective normalization factors in order to compare them on the same plot. The normalized scalar concentrations are compared to the normalized experimental data for the first and second spectrometer setups in Figures 43 and 44, respectively.

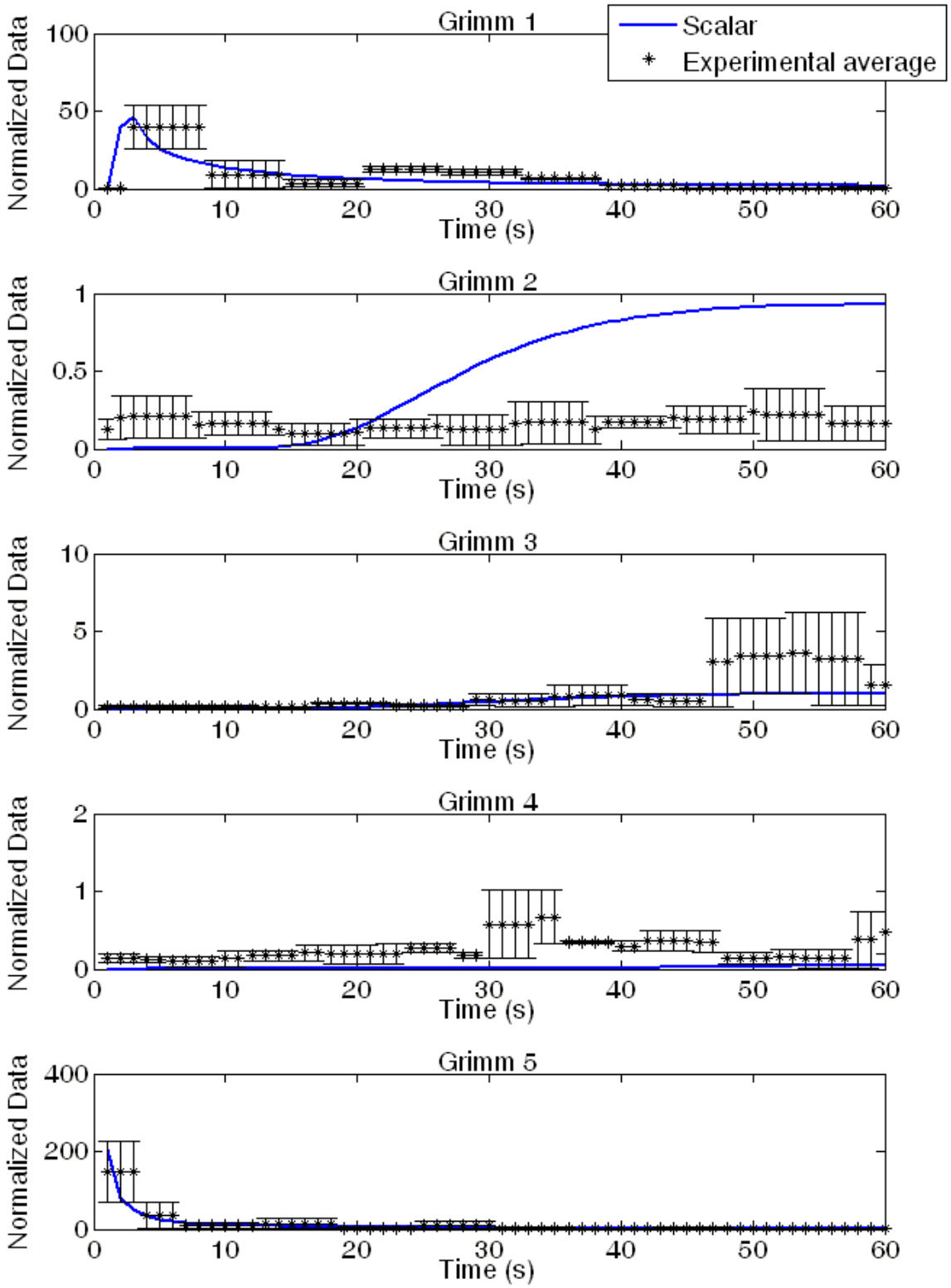

Figure 44: Normalized scalar and experimental data comparison at each Grimm spectrometer location for setup #1.

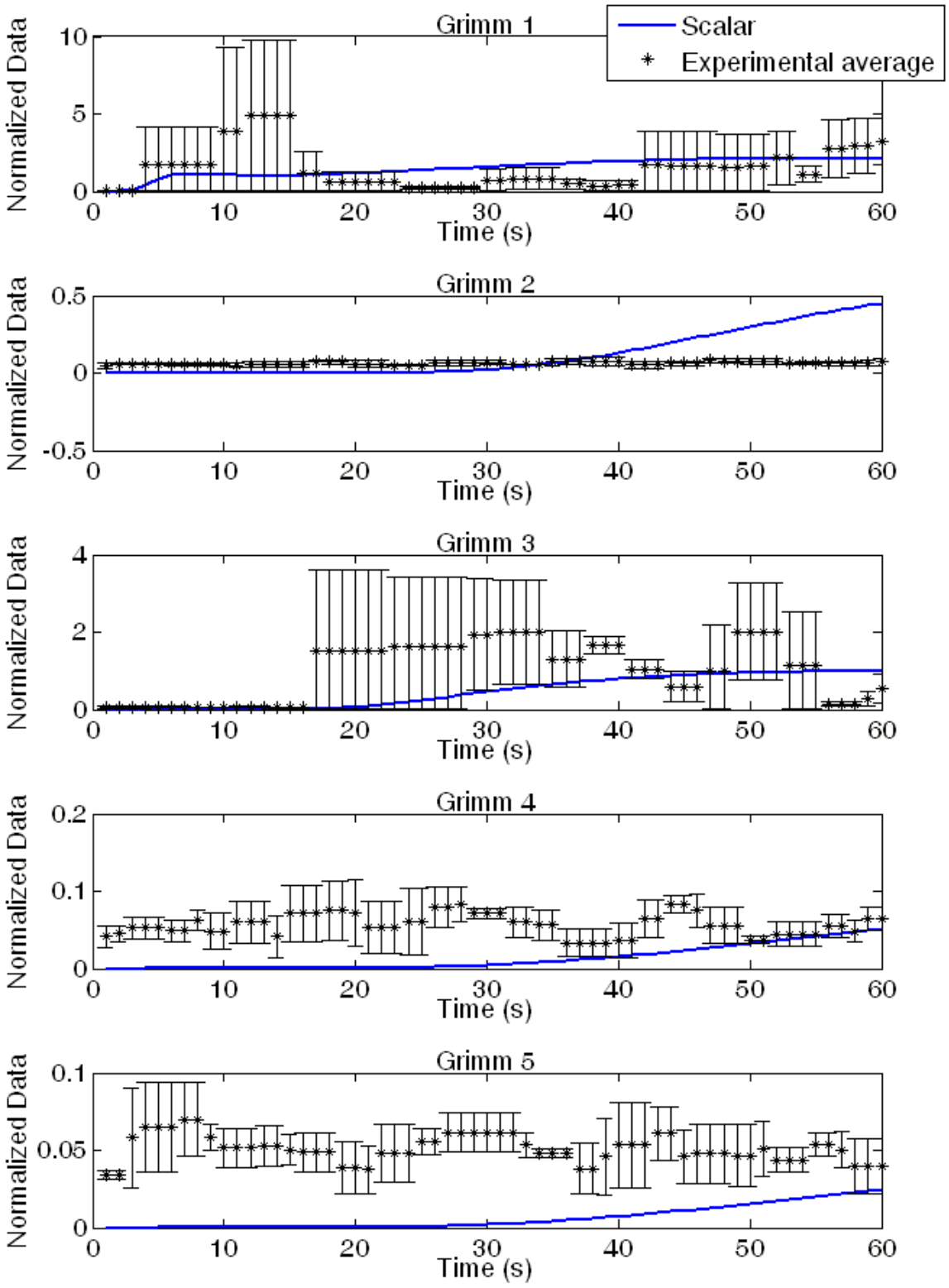

Figure 45: Normalized scalar and experimental data comparison at each Grimm spectrometer location for setup #2.

Chapter 6: Conclusions

The feasibility and mechanisms of airborne spread of the influenza virus among human subjects has been thoroughly examined from an engineering perspective in this study. Employing the use of various CFD techniques and software, the transport of tiny particles that may contain this virus has been modeled in great detail, from the smaller scale of a single droplet of sputum and the effects of different constituents within the droplet, to the larger scale of "clouds" containing thousands of particles dispersing inside of a room.

Starting with the simple case of a pure water droplet, evaporating (or growing due to condensation) in air of a constant temperature, relative humidity, and velocity, we then built upon this model, step by step, until finally realizing our goal—the creation of a sophisticated, precise model of a droplet with the properties of sputum, introduced into a turbulent, buoyant jet, which is issuing into (and mixing with) stagnant ambient surroundings. This model has been proven to be quite accurate at predicting the properties of binary aqueous solution droplets containing either sodium chloride, glucose, or bovine serum albumin. For ternary or higher order solutions, it is difficult to assess with certainty the accuracy of the model, as there is little experimental data available pertaining to solutions of interest. For humidity above 85% the model can predict properties of glucose + NaCl + water systems exceptionally well, but no experimental data for this system could be found below this humidity for validation. For solutions of NaCl + BSA + water our model compares reasonably well with the experimental data, though the error increases as the NaCl/BSA ratio moves closer to 1, apparently due to an

interaction between the solutes that is not included in the model. There is a definite need for more experimental work to determine the properties of multi-component droplets of biological significance under different conditions.

In the second part of this study, the spread of coughed droplets within a room was simulated in two different ways and compared with data from experiments performed at the Morgantown NIOSH facility. The particle injection method seems to compare fairly well with Grimms 1 and 5 in the first setup, but no particles were captured the entire 60 seconds at the other spectrometer locations. This can be justified for Grimms 2 and 4 by assuming the experimental data is just noise, but Grimm 3 seems a bit too high towards the end of the 60 seconds to be excused as being solely background noise. The second setup proved much more difficult to match the particle simulation with experiments, since there were no longer any Grimms directly on the axis of the inlet. By increasing the virtual volume of the spectrometers in the particle trapping code, we were able to obtain counts in the range of the experiments, though the trends of the data do seem to err significantly from the experiments in some areas. The scalar simulation seems to compare well with the experiments, perhaps even better than the particle simulation, however it must be pointed out that Figures 43 and 44 are linearly scaled, while Figures 41 and 42 are log scale. Overall, it can be said that the scalar behaves more like an average, or perhaps like a spline interpolation of the experimental data. The trend of the scalar is much smoother than that of the particle simulation, which suggests that it is less accurate at predicting sudden “jumps” or “dips” in the data at particular locations and times.

References

Andreas, E. L, 1989: Thermal and size evolution of sea spray droplets. CRREL Rep. 89-11, U. S. Army Cold Regions Research and Engineering Laboratory, 37 pp. (NTIS: ADA210484.)

Andreas, E.L., 2005: Handbook of Physical Constants and Functions for Use in Atmospheric Boundary Layer Studies. ERDC/CRREL M-05-1

Archer, R.J., La Mer, V., 1955: The Rate of Evaporation of Water Through Fatty Acid Monolayers. J. Phys. Chem., Vol. 59, pp. 200-208

Bejan, A., 2004: Convection Heat Transfer, 3rd edition. Wiley, 694 pp.

Benbough, J.E., 1969: The Effect of Relative Humidity on the Survival of Airborne Semliki Forest Virus. J. gen. Virol., Vol. 4, pp. 473-477

Benbough, J. E., 1971: Some Factors Affecting the Survival of Airborne Viruses. J. gen. Virol., 10, 209-220

Bjørn, E. and Nielsen, P.V., 2002: Dispersal of exhaled air and personal exposure in displacement ventilated rooms. Indoor Air, Vol. 12, pp. 147-164

Buck, A.L., 1981: New equations for computing vapor pressure and enhancement factor. J. Applied Meteorology, Vol. 20, pp. 1527-1532

Carey, V.P., 2007: Liquid Vapor Phase Change Phenomena. Taylor and Francis, 600 pp.

Chao, C.Y.H., Wan, M.P., Morawska, L., Johnson, G.R., Ristovski, Z.D., Hargreaves, M., Mengersen, K., Corbett, S., Li, Y., Xie, X., Katoshevski, D., 2009: Characterization of expiration air jets and droplet size distributions immediately at the mouth opening. Aerosol Sci., Vol. 40, pp. 122-133

Clift, R., Gauvin, W.H., 1970: The motion of particles in turbulent gas streams. Proc. Chemeca 70, 1, pp. 14-28

Cohen, M.D., Flagan, R.C., Seinfeld, J.H., 1987: Studies of Concentrated Electrolyte Solutions Using the Electrodynamic Balance. J. Phys. Chem., Vol. 91, pp. 4583-4590

Comesaña, J.F., Correa, A., Sereno, A., 1999: Measurements of Water Activity in "Sugar" + Sodium Chloride + Water Systems at 25 C. J. Chem. Eng. Data, Vol. 44, pp. 1132-1134

Crowe, C. T., Sommerfeld, M., and Tsuji, Y., 1997: Multiphase Flows with Droplets and Particles. CRC Press, 471 pp.

Duguid JP 1946. The size and duration of air-carriage of respiratory droplets and droplet nuclei. The Journal of Hygiene Vol 44 (6), pp 471-479

FLUENT INC., 2001: FLUENT 6.0 Documentation

Frenkiel, J., 1965: Evaporation Reduction: Physical and chemical principles and review of experiments. Unesco, 79 pp.

Inouye, S., Matsudaira, Y., and Sugihara, Y., 2006: Masks for Influenza Patients: Measurement of Airflow from the Mouth. Jpn. J. Infect. Dis., 59, 179-181

Iwata, S., Lemp, M.A., Holly, F.J., Dohlman, C.H., 1969: Evaporation rate of water from the precorneal tear film and cornea in the rabbit. Investigative Ophthalmology, Vol. 8, No. 6, pp. 613-619

Kreidenweis, S.M., Koehler, K., DeMott, P.J., Prenni, A.J., Carrico, C., Ervens, B., 2005: Water activity and activation diameters from hygroscopicity data - Part 1: Theory and application to inorganic salts. Atmos. Chem. Phys., 5, 1357-1370

Langmuir, I., 1917: The Constitution and Fundamental Properties of Solids and Liquids II. J. Amer. Chem. Society, Vol. 39, pp. 1848-1906

Law, A. W. K., Wang, H. W., and Herlina, 2003: Combined Particle Image Velocimetry/Planar Laser Induced Fluorescence for Integral Modeling of Buoyant Jets. J. Engr. Mech., Vol. 129, No. 10, 1189-1196

Lester, W., Jr., 1948: The Influence of Relative Humidity on the Infectivity of Air-borne Influenza A Virus (PR8 Strain). Dept. of Med., University of Chicago, 361-368

Lin, D.Q., Zhu, Z.Q., Mei, L.H., Yang, L.R., 1996: Isopiestic Determination of the Water Activities of Poly(ethyleneglicol) + Salt + Water Systems at 25 °C. J. Chem. Eng. Data, Vol. 41, pp. 1040-1042

Lovelock, J. E., 1957: The Denaturation of Lipid-Protein Complexes as a Cause of Damage by Freezing. Proceedings of the Royal Society of London. Series B, Biological Sciences, Vol. 147, No. 929, pp. 427-433

Lowen, A.C., Mubareka, S., Tumpey, T.M., Garcia-Sastre, A., Palese, P., 2006: The guinea pig as a transmission model for human influenza viruses. PNAS, vol 103, no. 26, pp.9988-9992

Lozato, P.A., Pisella, P.J., Baudouin, C., 2001: Phase lipidique du film lacrymal: physiologie et phatologie. J. Fr. Ophtalmol., Vol. 6, pp. 643-658

Majima, Y., Harada, T., Shimizu, T., Takeuchi, K., Sakakura, Y., Yasuoka, S., Yoshinaga, S., 1999: Effect of Biochemical Components on Rheologic Properties of Nasal Mucus in Chronic Sinusitis. Am. J. Respir. Crit. Care Med., Vol. 160, pp. 421-426

Mansour, H., Wang, D., Chen, C., Zografi, G., 2001: Comparison of Bilayer and Monolayer Properties of Phospholipid Systems Containing Dipalmitoylphosphatidylglycerol and Dipalmitoylphosphatidylinositol. Langmuir 2001, 17, pp. 6622-6632

Medical Ecology.org and White, J., 2004: Influenza. http://www.medicalecology.org/diseases/influenza/influenza.htm

Mikhailov, E., Vlasenko, S., Niessner, R., and Poschl, U., 2004: Interaction of aerosol particles composed of protein and salts with water vapor: hygroscopic growth and microstructural rearrangement. Atmos. Chem. Phys., 4, 323-350

Morawska, L., 2006: Droplet fate in indoor environments, or can we prevent the spread of infection? Indoor Air 2006; 16: 335-347

Mudgil, P., Torres, M., Millar, T.J., 2006: Adsorption of lysozyme to phospholipid and Meibomian lipid monolayer films. Colloids and Surfaces B: Biointerfaces, Vol. 48, pp. 128-137

Murphy FA, Kingsbury DW. Virus taxonomy. In: Fields BN, Knipe DM, editors. Fundamental virology. 2nd ed. New York: Raven Press; 1991. p. 9-35

Peng, C., Chow, A.H.L., Chan, C., 2000: Hygroscopic study of glucose, citric acid and sorbitol using an electrodynamic balance: comparison with UNIFAC predictions. Aerosol Sci. Tech. 35, pp. 753-758

Polozov, I.V., Bezrukov, L., Gawrisch, K., Zimmerberg, J., 2008: Progressive ordering with decreasing temperature of the phospholipids of influenza virus. Nature Chem. Bio., Vol. 4, pp. 248-255

Pruppacher, H. R., and J. D. Klett, 1978: Microphysics of Clouds and Precipitation. D. Reidel, 714 pp.

Samet, J.M., Cheng, P.W., 1994: The Role of Airway Mucus in Pulmonary Toxicology. Environmental Health Perspectives, Vol. 102, Supp. 2, pp. 89-103

Schaffer, F. L., Soergel, M. E., and Straube, D. C., 1976: Survival of Airborne Influenza Virus: Effects of Propagating Host, Relative Humidity, and Composition of Spray Fluids. Archives of Virology, 51, 263-273

Schrader, W., Ebel, H., Grabitz, P., Hanke, E., Heimburg, T., Hoeckel, M., Kahle, M., Wente, F., Kaatze, U., 2002: Compressibility of Lipid Mixtures Studied by Calorimetry

and Ultrasonic Velocity Measurements. J. Phys. Chem. B, Vol. 106, No. 25, pp. 6581-6586

Scott, H.L., Lee, C.Y., 1980: The surface tension of lipid water interfaces: Monte Carlo simulations. J. Chem. Phys., Vol. 73, No. 10, pp. 5351-5353

Smirnov, A., Shi, S., Celik, I., 2001: Random Flow Generation Technique for Large Eddy Simulations and Particle-Dynamics Modeling. J. Fluids Engr., Vol. 123, pp. 359-371

Sobsey, M. D., and Meschke, J. S., 2003: Virus Survival in the Environment with Special Attention to Survival in Sewage Droplets and Other Environmental Media of Fecal or Respiratory Origin. 1-87

Spicer, S.S., and Martinez, J.R., 1984: Mucin Biosynthesis and Secretion in the Respiratory Tract. Env. Health Perspectives, Vol 55, pp. 193-204

Stallknecht, D.E., Kearney, M.T., Shane, S.M., Zwank, P.J., 1990: Effects of pH, Temperature, and Salinity on Persistence of Avian Influenza Virues in Water. Avian Diseases, Vol. 34, No.2. (Apr.-Jun., 1990), pp. 412-418

Sun, W., Ji, J., 2007: Transport of Droplets Expelled by Coughing in Ventilated Rooms. Indoor Build Env., Vol. 16, No. 6, pp. 493-504

Sun., W., Ji, J., Li, Y., Xie, X., 2007: Dispersion and settling characteristics of evaporating droplets in ventilated room. Building and Env., Vol. 42, pp. 1011-1017

Tanaka, Y., Takei, T., Aiba, T., Masuda, K., Kiuchi, A., Fujiwara, T., 1986: Development of synthetic lung surfactants. J. Lipid Research, Vol. 27, pp. 475-485

Tang, I.N., 1996: Chemical and size effects of hygroscopic aerosols on light scattering coefficients. Journal of Geophysical Research, Vol 101, No. D14, pp. 19,245-19,250

Tang, I.N., 1979: Deliquesence Properties and Particle Size Change of Hygroscopic Aerosols. U.S. Department of Energy and Environment, 21 pp.

Tang, J. W., Li, Y., Eames, I., Chan, P. K. S., and Ridgway, G. L., 2006: Factors involved in the aerosol transmission of infection and control of ventilation in healthcare premises. J. Hosp. Infection, 64, 100-114

Tang, J.W. and Settles, G.S., 2008: Images in Clinical Medicine: Coughing and Aerosols. New England J. Med., Vol. 359, No. 15

Tellier, R., 2006: Review of Aerosol Transmission of Influenza A Virus. Emerging Infectious Diseases, Vol. 12 No. 11, pp. 1657-1662

Wan, M.P. and Chao, C.Y.H., 2007: Transport Characteristics of Expiratory Droplets and Droplet Nuclei in Indoor Environments With Different Ventilation Airflow Patterns. J. Biomech. Engr., Vol. 129, pp. 341-353

Wang, H.W., and Law, A.W. K., 2002: Second order integral model for a round turbulent buoyant jet. J. Fluid Mech., 459, 397–428

Williams, M.M.R., Loyalka, S.K., 1991: Aerosol Science Theory and Practice. Pergamon Press, 466 pp.

Wustneck, R., Perez-Gil, J., Wustneck, N., Cruz, A., Fainerman, V.B., Pison, U., 2005: Interfacial properties of pulmonary surfactant layers. Advances in Colloid and Interface Science, Vol. 117, pp. 33-58

Xie, X., Li, Y., Chwang, A.T.Y., Ho, P.L., Seto, W.H., 2007: How far droplets can move in indoor environments - revisiting the Wells evaporation-falling curve. Indoor Air, Vol. 17, pp. 211-225